

Quantum-optical description of photon statistics and cross correlations in high-order harmonic generation

Ákos Gombkötő¹, Péter Földi^{1,2} and Sándor Varró^{2,3}

¹*Department of Theoretical Physics, University of Szeged, Tisza Lajos körút 84, H-6720 Szeged, Hungary*

²*ELI-ALPS, ELI-HU Non-profit Ltd., Wolfgang Sandner utca 3, H-6728 Szeged, Hungary*

³*Wigner Research Centre for Physics, Konkoly-Thege M. út 29-33, H-1121 Budapest, Hungary*

 (Received 11 April 2020; revised 14 November 2020; accepted 26 August 2021; published 7 September 2021)

We present a study of photon statistics associated with high-order harmonic generation (HHG) involving one-mode and intermodal correlations of the high harmonic photons. The aim of the paper is to give insight into the nonclassical properties of high-order harmonic modes. To this end, we use a simplified model describing an elementary quantum emitter: the model of a two-level atom. While the material system is extremely simplified in this description, the conclusions and the methods may be generalized for more complex cases. Our primary interest is an effective model of HHG in which the exciting pulse is classical and the harmonics are quantized, although we touch upon the more generalized, fully quantized model as well. Evolution of the Mandel parameter, photon antibunching, squeezing, and cross correlations are calculated. Results imply that with respect to a single quantized emitter, nonclassicality of the harmonics is present: sub-Poissonian photon statistic and squeezing can characterize certain optical modes, while strong anticorrelation can also be present.

DOI: [10.1103/PhysRevA.104.033703](https://doi.org/10.1103/PhysRevA.104.033703)

I. INTRODUCTION

High-order harmonic generation (HHG) is a strongly nonlinear effect that is observed in several state-of-the-art experiments [1–3]. One of the most important applications is the generation of attosecond pulses, which can monitor or induce physical processes on an experimentally unprecedented timescale [4,5]. Therefore, deep understanding of the physical mechanisms underlying the phenomenon of HHG is of crucial importance.

Usually, the calculations involved in strong-field physics and attosecond science are based on the semiclassical approach, treating the electron quantum mechanically and the electromagnetic field classically [6–8].

On the other hand, quantized description of various phenomena in strong fields has already been discussed in the early 1980s. Reference [9] gives a nonperturbative treatment of HHG in the nonlinear Compton process using a fully quantized framework [10]. More recently, the idea that the photon number distribution of a laser pulse shows fingerprints of the generation of high-order harmonics after the interaction with matter appeared in a theoretical paper [11]. Later on, the effect has been demonstrated both with gaseous [12] and solid-state targets [13]. A short review of quantum-optical spectrometry is contained in [14]. On the theoretical side, a general perturbative treatment of the problem has been given in [15].

In the most widely used picture that describes gaseous targets, the continuum energy levels and the charge acceleration play an important role [8]. However, for solid-state targets, it is possible for only bound states to be populated during the process [16], and even the two-level approximation can be valid for quantum wells [17]. Previous works highlight how a driven two-level system can model the properties ob-

served in HHG spectra [18–22]. Let us note that a model with finite number of bound states can directly be related to the harmonic generation of solid-state targets described in the velocity gauge using single-particle and dipole approximations. Then all transitions are interband; that is, the dynamics of states with different \mathbf{k} eigenvalues are independent [23,24].

An interesting experimental aspect of HHG is the possibility of performing photon counting experiments. In order to obtain exact photon statistics, one should calculate all higher-order correlation functions, but the experimentally most significant terms are those of up to second order [25].

Of particular interest are the intermodal cross-correlation functions, the calculation of which is generally nontrivial. The properties of the two-mode correlation function are connected with the characterization of the electromagnetic field as a whole, which, as a first approximation, can be done by measuring second-order intermode cross correlations.

Naturally, quantum-optical properties like photon statistics are inherently unobtainable from a semiclassical approach. Although there have been numerous studies—both experimental and theoretical—about the photon statistics of second- and N th-order harmonics [26,27], fully quantum-optical treatments of the HHG are relatively rare.

The quantum properties of the radiation by an isolated, pointlike system may be affected for example by the following properties: the structure of the relevant energy levels of the system and modes, and the transition dipole moments; the polarization, intensity, and quantum properties (photon statistics) of the excitation; the timescale of the harmonic generation, i.e., whether spontaneous emission plays a role in the dynamics.

In this paper, we will only deal with strong, coherent excitation and its interaction with a two-level system, on a

timescale that is short compared to the characteristic time of the spontaneous emission.

The paper is organized in the following way. In Sec. II we give definitions of the correlation functions and other quantities calculated in this article. Section III specifies the model [21] we investigate. In Sec. IV we present semianalytic and numerical results connected to the photon statistics of high-order harmonics induced by classical radiation, while the intermodal correlations are treated in Sec. V. As an outlook, we give a brief presentation of results concerning the quantized excitation in Sec. VI. Conclusions are given in Sec. VII.

II. CORRELATION FUNCTIONS

The complete characterization of the radiation field in terms of intensity is only possible in limited cases. More accurate descriptions are possible by using a hierarchy of correlation functions as defined by optical coherence theory [25,28,29].

Correlation functions provide a concise method for expressing the degree to which two (or more) dynamical properties are correlated. Generally speaking, the response of a system to a specific weak probe is often directly related to a correlation function; therefore, the determination of specific correlation functions have been the focus of many experimental settings and theoretical investigations [30,31].

In quantum-optical experiments, the most relevant auto- and cross-correlation functions are between photon numbers. Usually, semiconductor avalanche photodiodes are used as detectors in these experiments [32]. These detectors typically can achieve time resolution of the order of 500–50 ps. Since detectors typically average over the detection time, fast fluctuations of the correlation function (which can contain important information concerning the physics of ultrafast processes) are blurred. In recent years, picosecond resolution has become possible [33,34].

Below, we introduce quantities relevant to quantum-optical experiments. The experimental setup to measure these quantities is typically similar to that of Hanbury Brown and Twiss [35].

Mandel Q parameter:

$$Q_n(t) \equiv \langle N_n(t) \rangle (g_n^2(t, 0) - 1) = \frac{(\Delta N_n)^2}{\langle N_n \rangle} - 1.$$

Whenever it takes negative values, the photon statistics is called sub-Poissonian and can be called nonclassical [36]. We note that, during the time evolution, there can be time instants when the photon number expectation value becomes (exactly or numerically) zero. This circumstance can cause difficulties during numerical evaluations of Q_n .

The definition of the Q parameter is related to the second-order coherence function $g_n^2(t, \tau)$, specifically for the one-time $\tau = 0$ case. The second-order coherence function

$$g_i^2(t, \tau) \equiv \frac{\langle a_i^\dagger(t) N_i(t + \tau) a_i(t) \rangle}{\langle N_i(t) \rangle \langle N_i(t + \tau) \rangle} \sim \frac{P(t + \tau | t)}{P(t + \tau)}$$

is related to the conditional probability $P(t + \tau | t)$ of a detector measuring a second photon at time $t + \tau$, granted that a first photon was measured at t .

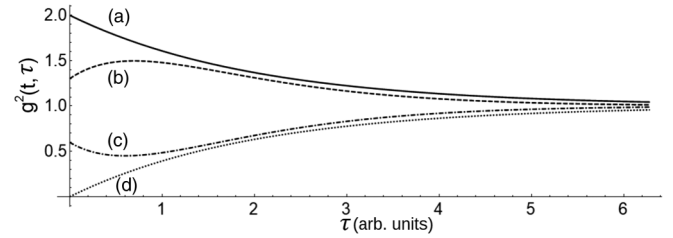


FIG. 1. Two-time correlation functions with fixed t . (a) super-Poissonian bunching, (b) super-Poissonian antibunching, (c) sub-Poissonian bunching, and (d) sub-Poissonian antibunching.

Photon antibunching measure:

$$\delta g_i^2(t, \tau) \equiv \lim_{\tau \rightarrow 0} \frac{g_i^2(t, \tau) - g_i^2(t, 0)}{\tau}. \quad (1)$$

Definitions and quantifications of photon bunching and antibunching are not completely unambiguous in the literature. Especially in experimental situations, when one considers the integration of signals by the detector, the concept of bunching needs careful handling [26,37–41]. For the sake of clarity, we list the commonly used definitions of photon antibunching for a single mode.

The presence of photon antibunching is equivalent to (Def. 1) $g_n^2(t, 0) < 1$ or $Q(t) < 0$ [42], (Def. 2) $G_n^2(t, \tau) > G_n^2(t, 0)$, where the quantities are defined by $G_n^2(t, \tau) = \langle a_n^\dagger(t) a_n^\dagger(t + \tau) a_n(t + \tau) a_n(t) \rangle$ [25], and (Def. 3) $g_n^2(t, \tau) > g_n^2(t, 0)$ [41].

Comparison of possible definitions are discussed in [26,43–45]. We have used antibunching according to (Def. 3), similar to [46]. Illustrative cases are presented in Fig. 1. The positivity of $\partial_\tau g^2(t, \tau)|_{\tau=0}$ implies (assuming that photon absorption happened at time t) that the probability of photon absorption is larger some small τ time later than the simultaneous absorption of two photons.

Intermodal cross correlation for two modes:

$$g_{ij}^2(t) = \frac{\langle N_i(t) N_j(t) \rangle}{\langle N_i(t) \rangle \langle N_j(t) \rangle}.$$

The field is nonclassical, if the inequality $g_{ii}^2(t) g_{jj}^2(t) < [g_{ij}^2(t)]^2$ stands [47]. There are additional inequalities [45], but here we only consider the following one: specifically, nonclassical entanglement between two (i and j) modes is implied if the

$$\langle N_i N_j \rangle < |\langle a_i a_j^\dagger \rangle|^2$$

relation is fulfilled [48].

Another quantity of interest is the squeezing of the harmonic modes. Light is considered to be squeezed in a given mode if there exists a quadrature-variance smaller than the one associated with the vacuum state [49,50]. The minimal variance (and its associated phase) can be calculated through the smaller eigenvalue (and associated eigenvector) of the noise-ellipse matrix. To quantify it, we use the following notations: $X_n \equiv \frac{a_n^\dagger + a_n}{2}$, $Y_n \equiv i \frac{a_n^\dagger - a_n}{2}$, $X_{2n} \equiv \frac{a_n^2 + a_n^{\dagger 2}}{2}$, and $Y_{2n} \equiv i \frac{a_n^2 - a_n^{\dagger 2}}{2}$. Then the noise ellipse is

$$\begin{pmatrix} \langle (\Delta X)^2 \rangle & \frac{1}{2} \langle \{\Delta X, \Delta Y\} \rangle \\ \frac{1}{2} \langle \{\Delta X, \Delta Y\} \rangle & \langle (\Delta Y)^2 \rangle \end{pmatrix}, \quad (2)$$

where $\{\cdot, \cdot\}$ denotes the anticommutator. The eigenvalues [37,51] expressed with the above notations

are

$$\begin{aligned}\lambda_{\pm} &= \frac{1}{4}[\langle\{\Delta a, \Delta a^{\dagger}\}\rangle \pm 2|\langle(\Delta a)^2\rangle|] \\ &= \frac{1}{4}[1 + 2(\langle N \rangle - \langle X \rangle^2 - \langle Y \rangle^2) \pm 2|\langle X_2 + iY_2 \rangle - \langle X + iY \rangle^2|].\end{aligned}\quad (3)$$

The quantum state of a given mode is squeezed if $\lambda_{-} < \frac{1}{4}$.

III. MODEL

In our investigation, we assumed that the excitations are—at least before interaction—characterized by coherent states. The model of the material is a two-level system. The simplicity of two-level systems helps to form qualitatively (and sometimes quantitatively) correct predictions and offers insight into the dynamics of the HHG. Furthermore, the methods used in this article can be generalized to more complex high harmonic sources as well.

Although harmonic generation is a nonlinear optical effect, only relevant in high-field settings, the intensities of the harmonics are typically much lower than that of the excitation. Therefore, especially when investigating the “one-atom response,” the assumption of classicality for the scattered harmonic radiation might not be necessarily valid.

Let us consider the following Hamiltonian terms:

$$\begin{aligned}H_a &= \hbar \frac{\omega_0}{2} \sigma_z, \\ H_h &= \sum_{n \in HH} \hbar \omega_n a_n^{\dagger} a_n, \quad H_{ah} = \sum_{n \in HH} \hbar \frac{\Omega_n}{2} \sigma_x (a_n + a_n^{\dagger}), \\ H_e &= \sum_{n \in E} \hbar \omega_n a_n^{\dagger} a_n, \quad H_{ae} = \sum_{n \in E} \hbar \frac{\Omega_n}{2} \sigma_x (a_n + a_n^{\dagger}),\end{aligned}$$

where the first term corresponds to a two-level atom, with the operators σ_i being the Pauli matrices, the second (fourth) term describes the quantized scattered (excitation) electromagnetic modes, and the third (fifth) term expresses the interaction using dipole approximation. Summations over HH(E) refer to summation over modes of the high harmonics (excitation).

The general Hamiltonian, with both quantized harmonics and excitation, can be written as

$$H_{qq} = H_a + H_{ah} + H_h + H_{ae} + H_e. \quad (4)$$

Usually, it is assumed that the interaction of the pulse with matter changes the quantum statistics of the pulse only slightly. In our experience the backaction on the excitation, while noticeable, does not (at least for short interaction times) have significant effect on the dynamics of the dipole operator. For this reason, we will be utilizing the classical approximation of the excitation, leading to the following effective Hamiltonian [21]:

$$H_{qc}(t) = H_a + H_h + H_{ah} + H_{ex}(t), \quad (5)$$

where the electromagnetic field of the excitation can be described as

$$H_{ex}(t) = -DE(t) = -d\sigma_x E(t) = \hbar \frac{\Omega(t)}{2} \sigma_x. \quad (6)$$

We note that $\Omega_n = 2d\sqrt{\frac{\hbar\omega_n}{\epsilon_0 V}}$, where V is the quantization volume. Let us denote the eigenstates of the atomic Hamiltonian by $|e\rangle$ and $|g\rangle$, i.e., $H_a|e\rangle = \frac{\hbar\omega_0}{2}|e\rangle$ and $H_a|g\rangle = -\frac{\hbar\omega_0}{2}|g\rangle$.

In this model, in principle all the electromagnetic modes would need to be accounted for, with proper initial conditions.

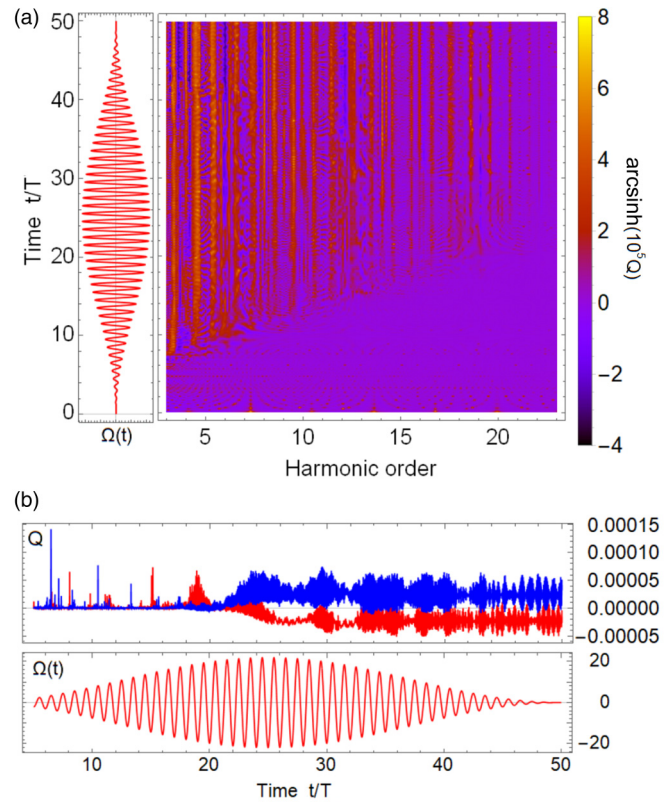


FIG. 2. Mandel parameter under pulsed excitation. Subfigure (a) shows $\sinh^{-1}(10^5 Q)$ on the central panel, with the (resonant) excitation on the left panel. Top panel of subfigure (b) shows time evolution of Q of an even (18th) harmonic with the ω_0/ω detuning being 0.8 (blue) and 1.2 (red), while the bottom panel shows the excitation.

For simplicity, in numerical calculations we assumed the initial condition to be $|\Psi(0)\rangle = |g\rangle \otimes |0\rangle \otimes \dots \otimes |0\rangle$.

The dynamics of the high-order harmonics are induced by the quantized dipole driven by strong classical and weak quantized fields. For practical reasons, we need to utilize some kind of approximation for the calculations.

While the semiclassical theory of radiation assumes that the atomic quantities and field quantities are independent [52], i.e., $\langle\sigma_i a_j\rangle = \langle\sigma_i\rangle\langle a_j\rangle$, that assumption is clearly unacceptable when one investigates correlation functions.

On the other hand, it is true that the effect of the low-intensity high-harmonic radiation on a classically driven dipole—and thus on each other—is weak. The cumulative effects of the mode-mode interactions become palpable at the timescale of the spontaneous emission lifetime. Since in experimental settings the pulse is in the order of femtoseconds, we will neglect the interplay between different harmonics and consider the high harmonic modes independently.

We will treat the cases of monochromatic and pulsed excitations separately, with both assumed to be linearly polarized. The pulsed excitations have an electric field:

$$E(t) = A \sin^2(\omega_e t) \sin(\omega_f t + \phi) \quad \text{if } t \in [0, \pi/\omega_e], \\ 0 \quad \text{otherwise,}$$

where A denotes the amplitude, ϕ is the carrier envelope phase, and $\omega_e \ll \omega_f$ is fulfilled.

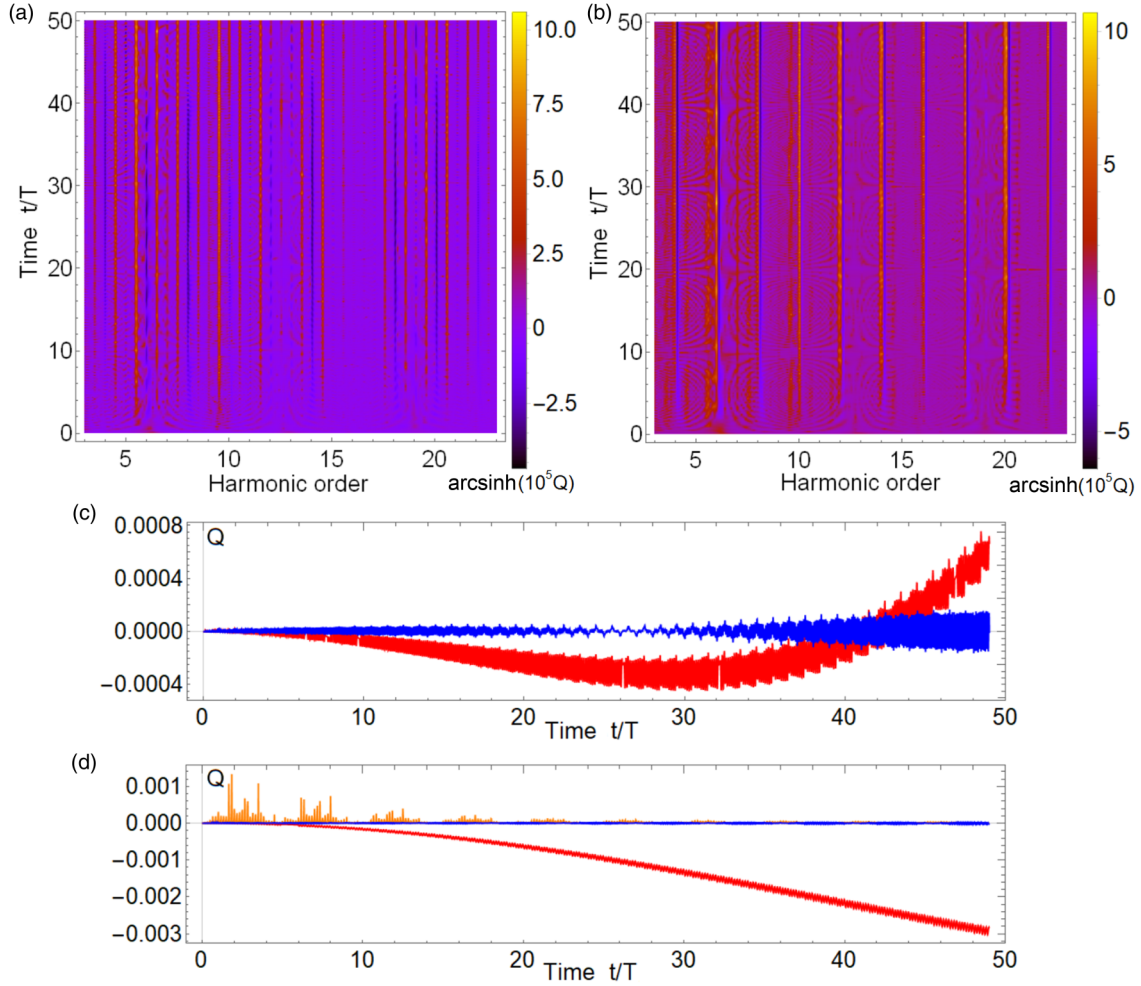


FIG. 3. Mandel parameter under monochromatic excitations. The parameters are chosen such that $\delta\omega = 0$ on subfigures (a) and (c) and $\delta\omega = 0.1\omega$ on subfigures (b) and (d). Subfigures (a) and (b) show evolution of the rescaled Mandel parameter $\sinh^{-1}(10^5 Q)$. Subfigures (c) and (d) show time evolution of the Mandel parameter of given odd-harmonic line (blue) and even harmonic line(s) (red and orange). The mode corresponding to the orange line has negligible population.

In this article, we use the following notations. Photon number operator: N_n ; atomic operators: $U = \sigma_x$, $V = -\sigma_y$, $W = \sigma_z$; first- and second-order field operators: $(a_n^\dagger + a_n)$, $i(a_n^\dagger - a_n)$, $(a_n^{\dagger 2} + a_n^2)$, $i(a_n^{\dagger 2} - a_n^2)$; first-order atom-field operators: $U_n^\pm = (i)^{(1\mp 1)/2} \sigma_x (a_n \pm a_n^\dagger)$, $V_n^\pm = -(i)^{(1\mp 1)/2} \sigma_y (a_n \pm a_n^\dagger)$, $W_n^\pm = (i)^{(1\mp 1)/2} \sigma_z (a_n \pm a_n^\dagger)$.

IV. ONE-MODE PROPERTIES

The harmonic spectrum is composed of odd-order harmonics and hyper-Raman lines (Mollow sidebands) which, in this paper, we call even-order harmonics in accordance with our earlier work [21]. To clarify our nomenclature, it is worth pointing out that these spectral lines correspond to Mollow triplets around the odd harmonics [53]. Since our focus is on strong-field excitations, the nonodd harmonic optical lines will be near to the spectral position of the even multiples of the base harmonics, so, for the sake of simplicity, we will call these (dual) lines even harmonics. We introduce the notation $\delta\omega$ for the spectral distance between the optical lines and the closest even-order multiple of the base harmonic. The actual value of delta omega is determined by the parameters of the excitation (amplitude, detuning). Further details can be found in Appendix A.

It can be argued [54] that harmonics should be defined based on the phase and carrier frequency (through χ^k nonlinear susceptibility) without reference to the position in the optical spectrum. From this argument, the radiation which we call even harmonics should be more precisely called odd harmonics disguised as even harmonics [55].

We note that, according to [56–58], results obtained for molecular targets suggest that the intensity of Mollow sidebands remain around the same order of magnitude as odd harmonics (in the macroscopic spectrum). They are also radiated at wider angles and therefore can be distinguished from the main harmonics, and in principle can also be isolated. It is important to note that recent experiments observed these hyper-Raman lines for atomic targets as well [59].

Starting from this section, we will present numerical results first, followed by the analytically gained ones, the mathematical background of which can be found in the Appendixes.

A. Mandel parameter

When we consider pulsed excitation, the photon statistic—just like the spectrum—becomes hard to characterize. The narrow peaks of the Mandel parameters at the early stage

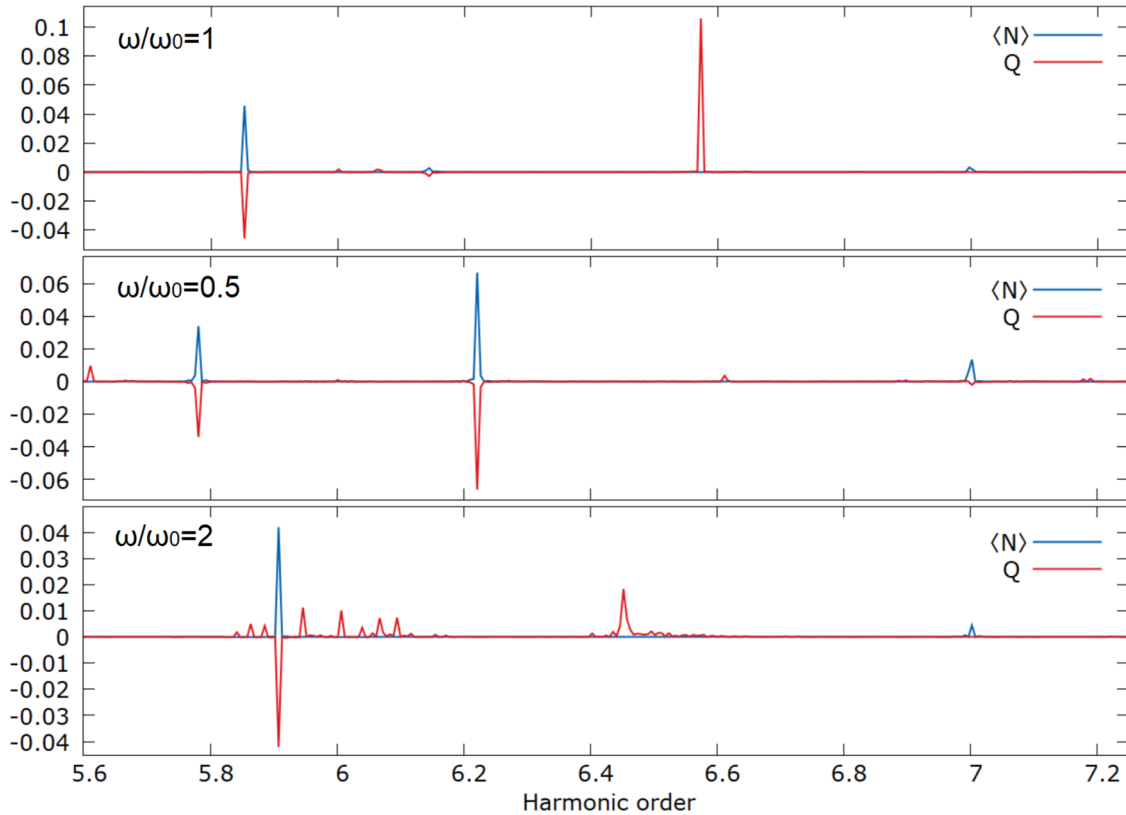


FIG. 4. Asymptotical averaged photon number expectation values (blue) and Mandel parameters (red) for resonant, red-detuned, and blue-detuned excitations. The horizontal axis is shared among the subfigures. The excitation is pulsed, with 25 optical cycle duration of rise and decay and 500 cycle duration of constant amplitude.

of the time evolution, visible in Fig. 2(b), are signatures of the initial transient effects. Then rapid oscillations appear, which have a considerably more regular pattern—that is, the average over multiple cycles is constant—when the pulse is over ($t > \tau$). Note that the detuning has a strong effect on the photon statistical properties in the case of pulsed excitations.

To make the analysis transparent, we present results specific to monochromatic excitations. We note that, in Fig. 3, the visible super-Poissonian modes (positioned between the harmonics) are characterized by very low photon-number expectation values, and their super-Poissonian quality can be considered a numerical artifact.

The Mandel parameters of odd harmonic modes usually display both positive and negative values within an optical cycle, being approximately zero on average. Even harmonic lines have more complicated behavior as follows.

(i) If $\delta\omega = 0$, the single even harmonic line will first become sub-Poissonian and then super-Poissonian [Fig. 3(c)]. An intuitive explanation is that this optical line develops significant squeezing (see Sec. IV B), while the photon-number mean value is only increasing moderately, rendering the photon-number fluctuation large as the interaction time increases.

(ii) If $|\delta\omega|$ is large, usually only one of the even-harmonic modes will be significantly populated, while the other spectral line develops significantly sub-Poissonian statistics [Fig. 3(d)]. Our calculation shows that $Q \approx -\langle N \rangle$, which is equivalent to $\langle N^2 \rangle \approx \langle N \rangle$; in other words, the photon statistic

of such an even harmonic mode is essentially a superposition of zero- and one-photon states.

These results imply that sub-Poissonian behavior is present in the even-harmonic (Hyper-Raman) lines. In order to check that our results remain valid for the case of higher photon numbers, we considered a very long, nearly monochromatic pulsed excitation.

Note that our earlier results in [21] were considerably less detailed. There, we only considered a single mode, while the excitation was pulsed, which did not offer as much transparency as the analysis of monochromatic excitation does.

We give the asymptotic value of Mandel parameters as a function of harmonic order, for a long “boxed” monochromatic excitation in Fig. 4. The excitation is 500 optical cycle long, with additional 25 cycle duration of rise and decay. In order to filter out the oscillations after the excitation, we took the average value over many cycles.

With respect to these averaged asymptotical values, we found our statements to be, up to a good approximation, valid. It is worth noting, however, that in these calculations the odd harmonics themselves could display super- or sub-Poissonian behavior, but, for them, the $|Q| \ll \langle N \rangle$ relation is fulfilled.

As we can observe, the presence of even-order harmonic (hyper-Raman line) modes with significant population (and nonclassicality) holds also for such pulsed excitations. As long as the rise and decay of the amplitude is relatively short, the sensitivity to the detuning is practically eliminated.

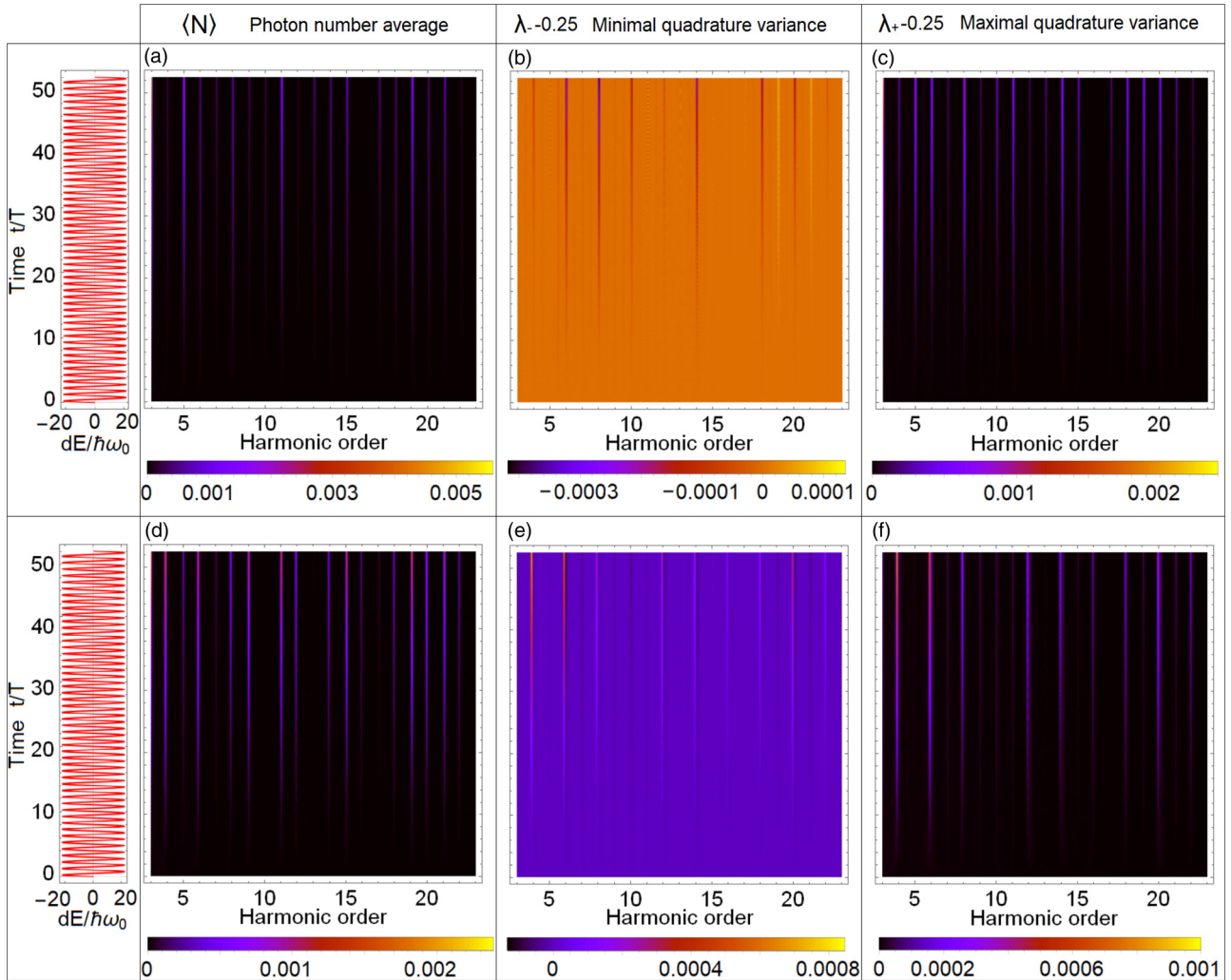


FIG. 5. Time evolution of field quantities. The upper and lower row of figures corresponds to two monochromatic excitations with slightly different amplitudes (shown in the left panels). Time evolution of $\delta\lambda_- - \frac{1}{4}$ is in subfigures (b) and (e), while $\delta\lambda_+ - \frac{1}{4}$ can be observed in subfigures (c) and (f). For the sake of clarity, we showed $\langle N \rangle$ in subfigures (a) and (d). Vertical axis is time measured in T ; horizontal axis is harmonic order. Amplitudes of the excitation have been chosen so that $\delta\omega = 0$ for (a) to (c) and $\delta\omega = 0.1\omega$ for (d), (e), and (f), corresponding to dimensionless amplitudes 21.2119 and 21.8354, respectively.

B. Time evolution of quadrature variance

The quadrature variance spectrum, that is, the value of the minimal and maximal variances λ_{\pm} in Eq. (3) as the function of the parameter ω_n , can display distinct properties depending on the chosen parameters, but it can be summarized in the following way.

The odd harmonics on the plateau display squeezing, which, however, is usually weak. The even harmonics have quantum properties that are very sensitive to the excitation parameters. If the parameters are chosen such that $\delta\omega$ is practically zero, particularly strong squeezing is present, among the even harmonics, whereas if $\delta\omega$ is large, strongly antisqueezed states ($\lambda_- > \frac{1}{2}$) will be produced, mainly in the more populated modes of the even harmonic lines. For illustration, we plotted relevant quantities in Fig. 5.

One may conclude that as far as producing squeezed states are concerned (obviously within the limits of this model) special attention is to be given to the parameter space for

which $\delta\omega = 0$ (for details, see the Appendixes). In such cases, the even harmonic lines display unusual behavior compared to other lines. The squeeze in these modes will grow faster than the photon number expectation values, rendering the photon statistics super-Poissonian beyond a given interaction time [see Fig. 3(c)].

C. Analytical approximation of photon statistics for extremal $\delta\omega$ values

Limiting ourselves to the case of monochromatic excitation, it is possible to give analytic insight into the resulting photon statistics of individual harmonics. Specifically, we focus on the special set of parameters that grant extremal $\delta\omega$.

Perturbative calculation in the fourth order, applied to the electromagnetic mode with ω_n angular frequency, leads us to the expression below. The b_2^e and b_2^s coefficients correspond to the (two-photon) components ($|e\rangle|2\rangle$ and $|g\rangle|2\rangle$) of the quantum state. The \mathcal{F} symbol denotes Fourier transform, while $\zeta_{1/2}$

are terms given in the Appendixes:

$$b_2^e(t)^{(4)} \approx -\frac{\Omega_n^2 t^2}{4\sqrt{2}} (\mathcal{F}\{b_0^e(0)[1 + i\zeta_1] - ib_0^g(0)\zeta_2\}(-\omega_n + \delta\omega) \mathcal{F}[1 - i\sigma_1](-\omega_n - \delta\omega) - e^{-i2\phi_0} \mathcal{F}\{b_0^g(0)[1 - i\zeta_1] - ib_0^e(0)\zeta_2^*\}(-\omega_n - \delta\omega) \mathcal{F}[i\zeta_2^*](-\omega_n - \delta\omega)), \tag{7}$$

$$b_2^g(t)^{(4)} \approx -\frac{\Omega_n^2 t^2}{4\sqrt{2}} (\mathcal{F}\{b_0^g(0)[1 - i\zeta_1] - ib_0^e(0)\zeta_2^*\}(-\omega_n - \delta\omega) \mathcal{F}[1 + i\zeta_1](-\omega_n + \delta\omega) - e^{i2\phi_0} \mathcal{F}\{b_0^e(0)[1 + i\zeta_1] - ib_0^g(0)\zeta_2\}(-\omega_n + \delta\omega) \mathcal{F}[i\zeta_2](-\omega_n + \delta\omega)). \tag{8}$$

The perturbative approach leads us to the following statements.

Odd harmonics. The quantum state of the field, up to the order presented, can be written as $|\Psi\rangle_{HH}^{(4)} \approx |0\rangle + \alpha|1\rangle + \alpha^2/\sqrt{2}|2\rangle$, where $\alpha \in \mathbb{C}$. By assuming that the coefficients follow a similar pattern at higher order, the quantum state of odd-order harmonics would be a coherent state with label $\alpha = \Omega_n/2\mathcal{F}[\zeta_2](-\omega_n \pm \delta\omega)t$. Naturally, the perturbative calculation is not strictly true. Predicted intensities are smaller than the numerically calculated values, but the nearly Poissonian (on the average) statistics is correctly reproduced.

Even harmonics. The quantum state of both hyper-Raman lines can be written as $|\Psi\rangle_{HH}^{(4)} \approx |0\rangle + \beta|1\rangle$, where, if we choose initial condition $|\Psi\rangle_a(0) = |g\rangle$, the β parameter is nonzero only for one even harmonic line, characterized by sub-Poissonian statistics. The $Q = -\langle N \rangle$ relation observed in numerical calculations follows straightforwardly, since $\langle N^2 \rangle = \langle N \rangle$.

D. Photon-bunching properties

By the definition that we use, photon (anti)bunching is implied by the sign of $\partial_\tau g^2(t, \tau)$. Expanding $g^2(t, t + \tau) - g^2(t, t)$ up to the first order in τ , we get

$$g^2(\tau) - g^2(0) \approx \tau \frac{\Omega \langle a^\dagger U^- a \rangle \langle N \rangle - \langle a^\dagger N a \rangle \langle U^- \rangle}{2 \langle N \rangle \langle N \rangle \langle N + \tau \frac{\Omega}{2} U^- \rangle}, \tag{9}$$

which can be simplified further. Since $\langle N \rangle > 0$ and $\langle a^\dagger N a \rangle > 0$ in the limit of small τ , the presence of photon bunching is determined by the sign and relative magnitude of $\langle U^- \rangle \propto \langle N \rangle$ and $\langle a^\dagger U^- a \rangle$.

The only significant dynamics that we observed—both for pulsed and monochromatic excitation—is the roughly $2\pi/\omega_n$ periodic photon antibunching. For most modes, the average value of δg is indistinguishable from zero, but for the sub-Poissonian even harmonic that has been plotted on Fig. 6, the average is slightly negative. Considering quantities averaged

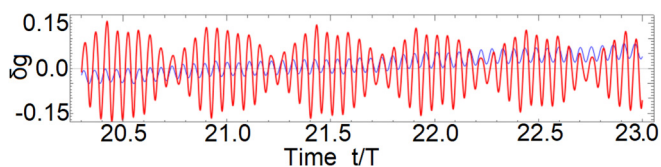


FIG. 6. Time evolution of photon-antibunching measure [Eq. (1)] of a given even harmonic mode (red), with the monochromatic excitation parameters chosen so that $|\delta\omega|$ is large. For the purpose of illustration we also show the rescaled and displaced mean photon value in blue.

over optical cycles, the fact that the sub-Poissonian statistic coincides with photon bunching can be interpreted as a consequence of the nonstationary state of the mode as the Mandel parameter decreases in time.

V. INTERMODE CORRELATION BETWEEN HARMONICS

A. Numerical results

As a first step of characterizing the radiation field as a whole, i.e., calculating the emerging cross correlations, the two-mode approximation proves to be useful.

First, we treat the case of monochromatic excitation, with parameters chosen so that $|\delta\omega| = 0$ and $|\delta\omega| = 0.1\omega$ is fulfilled. Results can be seen on Figs. 7 and 8, respectively.

Specifically for the $|\delta\omega| = 0$ parameter—which we can associate with particularly significant squeezing being present within the even harmonic modes—numerical results imply the following.

(i) Odd harmonic photons tend to be correlated with other odd harmonics, generally close to the classical limit (i.e., correlation of unit value).

(ii) Even and odd harmonic photons tend to be anticorrelated.

(iii) Even harmonic photons tend to be strongly correlated. This implies the theoretical possibility that HHG can be the source of wideband, correlated squeezed states.

For the $|\delta\omega| = 0.1\omega$ parameter—which is relatively close to the maximal $|\delta\omega|$ case, which we can associate with particularly nonclassical, nearly one-photon states being present within the even harmonic modes—numerical results imply the following.

(i) Odd harmonic photons tend to be correlated with other odd harmonics, generally close to the classical limit.

(ii) Even and odd harmonic photons tend to be significantly anticorrelated.

(iii) Even harmonic photons tend to be strongly anticorrelated. This implies the theoretical possibility that HHG can be the source of one-photon states in wide spectral ranges. We note that (at least in the cases investigated by us) the modes are more populated (the quantum states are closer to one-photon states) if the interaction time is longer and the coupling is stronger.

For pulsed excitation, the cross correlations become more complicated (see Fig. 9), but certain qualitative statements can be made as follows.

(i) Odd harmonic photons tend to be correlated with other odd harmonics, generally close to the classical limit.

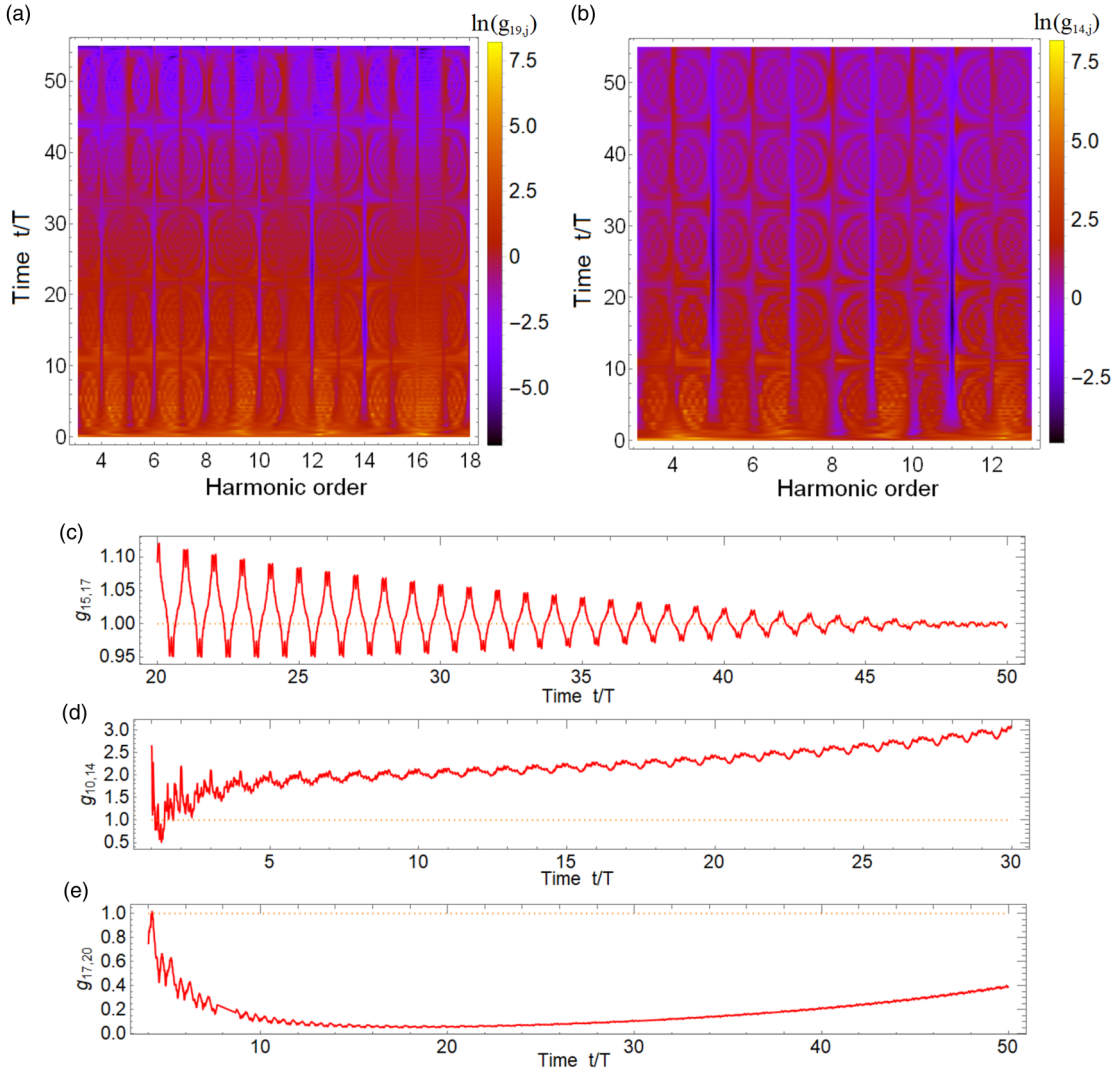


FIG. 7. Plot of cross-correlation functions for monochromatic excitation, with $\delta\omega = 0$. Subfigure (a) shows the time and frequency dependence of the two-mode correlation on logarithmic scale, where one of the modes is the 19th harmonic. (b) Same as in subfigure (a), but the fixed mode is the 14th harmonic. (c) Cross correlation between two odd (15th and 17th) harmonics. (d) Cross correlation between two even (10th and 14th) harmonics. (e) Cross correlation between odd and even (17th and 20th) harmonics.

(ii) Even and odd harmonic photons tend to be significantly anticorrelated.

(iii) Even harmonics photon's correlation with other even harmonic photons can be either stronger or weaker than the classical limit.

B. Analytical approximation of intermodal correlations for extremal $\delta\omega$ values

An approximate physical picture of the quantum state of the scattered radiation in the case of monochromatic exci-

tation can be constructed using analytic methods. As in the previous section, we will only consider the special cases of extremal $\delta\omega$.

Since our goal here is to gain a simple physical picture we will assume that the state of each electromagnetic mode spans a minimal space containing $|0\rangle$ and $|1\rangle$ photon number states, that is, we focus only on the terms with dominant contributions in intermodal cross correlations. For the sake of transparency, we will consider two electromagnetic modes (of arbitrary ω_1 and ω_2 , respectively). The quantum state can be written explicitly as

$$\begin{aligned}
 |\Psi\rangle = & U e^{-\frac{i}{\hbar}\epsilon+t} (b_{00}^e(t)|\tilde{e}\rangle|0\rangle|0\rangle + b_{01}^e(t)|\tilde{e}\rangle|0\rangle|1\rangle e^{-i\omega_2 t} + b_{10}^e(t)|\tilde{e}\rangle|1\rangle|0\rangle e^{-i\omega_1 t} + b_{11}^e(t)|\tilde{e}\rangle|1\rangle|1\rangle e^{-i(\omega_1+\omega_2)t}) \\
 & + U e^{-\frac{i}{\hbar}\epsilon-t} (b_{00}^g(t)|\tilde{g}\rangle|0\rangle|0\rangle + b_{01}^g(t)|\tilde{g}\rangle|0\rangle|1\rangle e^{-i\omega_2 t} + b_{10}^g(t)|\tilde{g}\rangle|1\rangle|0\rangle e^{-i\omega_1 t} + b_{11}^g(t)|\tilde{g}\rangle|1\rangle|1\rangle e^{-i(\omega_1+\omega_2)t}), \quad (10)
 \end{aligned}$$

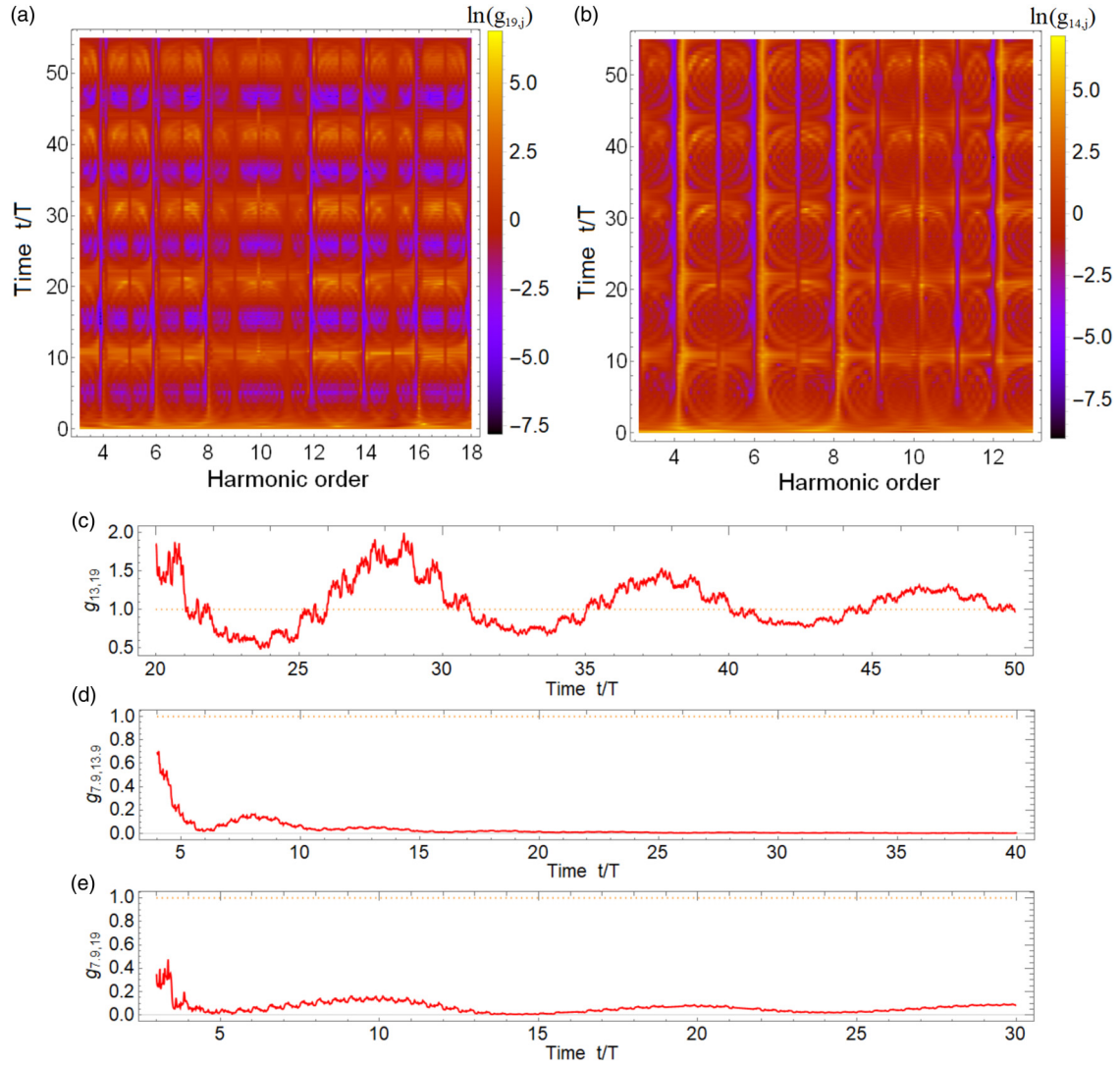


FIG. 8. Plot of cross-correlation functions for monochromatic excitation, with $\delta\omega = 0.1\omega$. Subfigure (a) shows the time and frequency dependence of the two-mode correlation on logarithmic scale, where one of the modes is the 19th harmonic. (b) Same as in subfigure (a), but the fixed mode is that of the 14th harmonic's more populated line. (c) Cross correlation between two odd (13th and 19th) harmonics. (d) Cross correlation between two more populated even (8th and 14th) harmonic lines. (e) Cross correlation between odd and even (8th and 19th) harmonics.

where $U \equiv e^{i\frac{A\xi}{2\omega}\sin(\omega t + \phi_0)\sigma_x} e^{i\frac{\omega t + \phi_0}{2}\sigma_z}$ (for details, see the Appendixes). We fix the initial condition so that, at time $t = 0$, $b_{lm}^g = b_{lm}^e = 0$ unless $l = m = 0$. The time evolution of the b coefficients is induced by

$$\hbar W(t) + \hbar(\sigma^+ e^{i(\omega t + \phi_0)} + \sigma^- e^{-i(\omega t + \phi_0)}) \left[\frac{\Omega_1}{2}(a_1^\dagger + a_1) + \frac{\Omega_2}{2}(a_2^\dagger + a_2) \right], \quad (11)$$

where $W(t)$ is defined by (A12). Below we give the perturbative results, neglecting second-order contributions of $\hbar W(t)$, and all nonresonant terms.

In first and second order, we get

$$b_{00}^e(t)^{(1)} = b_{00}^e(0)[1 + i\zeta_1(t)] - ib_{00}^g(0)\zeta_2(t), \quad (12)$$

$$b_{00}^g(t)^{(1)} = b_{00}^g(0)[1 - i\zeta_1(t)] - ib_{00}^e(0)\zeta_2^*(t), \quad (13)$$

$$b_{10}^e(t)^{(2)} = -i\frac{\Omega_1 t}{2} e^{-i\phi_0} \mathcal{F}\{b_{00}^g(0)[1 - i\zeta_1] - ib_{00}^e(0)\zeta_2^*\}(-\omega_1 - \delta\omega), \quad (14)$$

$$b_{10}^g(t)^{(2)} = -i\frac{\Omega_1 t}{2} e^{i\phi_0} \mathcal{F}\{b_{00}^e(0)[1 + i\zeta_1] - ib_{00}^g(0)\zeta_2\}(-\omega_1 + \delta\omega), \quad (15)$$

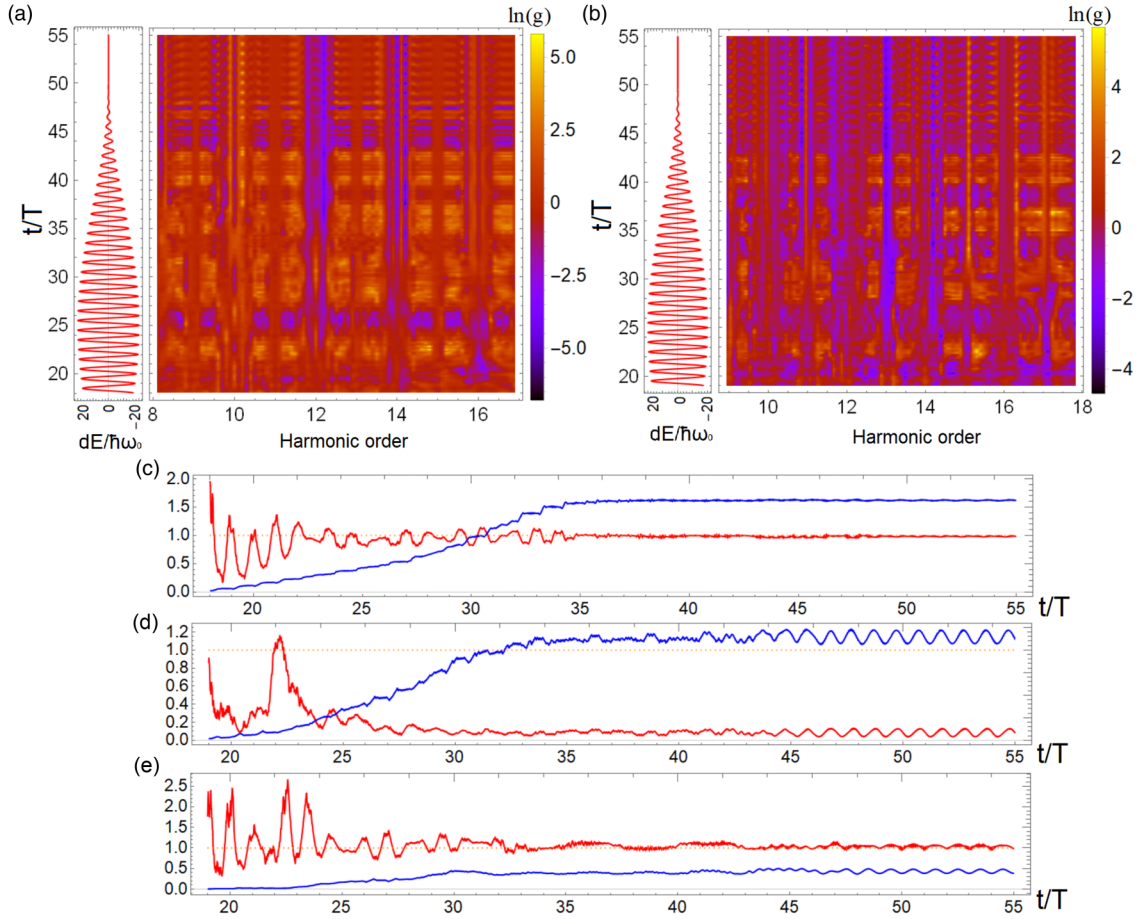


FIG. 9. Plot of cross-correlation functions for pulsed excitation. The left side shows the time dependence of the excitation in units of the optical cycles. (a) Logarithm of the cross correlation between the 17th mode and other optical modes. (b) Logarithm of the cross correlation between the 18th harmonic mode and other optical modes. (c)–(e) Cross-correlation function (red) and sum of ($10^4 \times$) photon number expectation values (blue) for 15th and 17th harmonics, 17th and 18th harmonics, and between two optical lines of the 18th harmonic, respectively.

$$b_{01}^e(t)^{(2)} = -i \frac{\Omega_{21} t}{2} e^{-i\phi_0} \mathcal{F}\{b_{00}^g(0)[1 - i\zeta_1] - ib_{00}^e(0)\zeta_2^*\}(-\omega_2 - \delta\omega), \quad (16)$$

$$b_{01}^g(t)^{(2)} = -i \frac{\Omega_{21} t}{2} e^{i\phi_0} \mathcal{F}\{b_{00}^e(0)[1 + i\zeta_1] - ib_{00}^g(0)\zeta_2\}(-\omega_2 + \delta\omega). \quad (17)$$

The most important third-order effect is that induced by $\hbar W(t)$, between the populations b_{10}^g , b_{10}^e and b_{01}^g , b_{01}^e , resulting in

$$b_{10}^e(t)^{(3)} \approx -i \frac{\Omega_{11} t}{2} (e^{-i\phi_0} \mathcal{F}\{b_{00}^g(0)[1 - i\zeta_1] - ib_{00}^e(0)\zeta_2^*\}(-\omega_1 - \delta\omega) [1 + i\zeta_1] - e^{i\phi_0} \mathcal{F}\{b_{00}^e(0)[1 + i\zeta_1] - ib_{00}^g(0)\zeta_2\}(-\omega_1 + \delta\omega) [i\zeta_2]), \quad (18)$$

$$b_{10}^g(t)^{(3)} \approx -i \frac{\Omega_{11} t}{2} (e^{i\phi_0} \mathcal{F}\{b_{00}^e(0)[1 + i\zeta_1] - ib_{00}^g(0)\zeta_2\}(-\omega_1 + \delta\omega) [1 - i\zeta_1] - e^{-i\phi_0} \mathcal{F}\{b_{00}^g(0)[1 - i\zeta_1] - ib_{00}^e(0)\zeta_2^*\}(-\omega_1 - \delta\omega) [i\zeta_2^*]), \quad (19)$$

$$b_{01}^e(t)^{(3)} \approx -i \frac{\Omega_{21} t}{2} (e^{-i\phi_0} \mathcal{F}\{b_{00}^g(0)[1 - i\zeta_1] - ib_{00}^e(0)\zeta_2^*\}(-\omega_2 - \delta\omega) [1 + i\zeta_1] - e^{i\phi_0} \mathcal{F}\{b_{00}^e(0)[1 + i\zeta_1] - ib_{00}^g(0)\zeta_2\}(-\omega_2 + \delta\omega) [i\zeta_2]), \quad (20)$$

$$b_{01}^g(t)^{(3)} \approx -i \frac{\Omega_{21} t}{2} (e^{i\phi_0} \mathcal{F}\{b_{00}^e(0)[1 + i\zeta_1] - ib_{00}^g(0)\zeta_2\}(-\omega_2 + \delta\omega) [1 - i\zeta_1] - e^{-i\phi_0} \mathcal{F}\{b_{00}^g(0)[1 - i\zeta_1] - ib_{00}^e(0)\zeta_2^*\}(-\omega_2 - \delta\omega) [i\zeta_2^*]). \quad (21)$$

Then, at the fourth order, we get

$$\begin{aligned}
 b_{11}^g(t)^{(4)} &\approx -\frac{\Omega_1\Omega_2t^2}{8}(\mathcal{F}\{b_{00}^g(0)[1-i\zeta_1]-ib_{00}^g(0)\zeta_2^*\}(-\omega_1-\delta\omega)\mathcal{F}[1+i\zeta_1](-\omega_2+\delta\omega) \\
 &\quad -e^{i2\phi_0}\mathcal{F}\{b_{00}^g(0)[1+i\zeta_1]-ib_{00}^g(0)\zeta_2\}(-\omega_1+\delta\omega)\mathcal{F}[i\zeta_2](-\omega_2+\delta\omega) \\
 &\quad +\mathcal{F}\{b_{00}^g(0)[1-i\zeta_1]-ib_{00}^g(0)\zeta_2^*\}(-\omega_2-\delta\omega)\mathcal{F}[1+i\zeta_1](-\omega_1+\delta\omega) \\
 &\quad -e^{i2\phi_0}\mathcal{F}\{b_{00}^g(0)[1+i\zeta_1]-ib_{00}^g(0)\zeta_2\}(-\omega_2+\delta\omega)\mathcal{F}[i\zeta_2](-\omega_1+\delta\omega)), \tag{22} \\
 b_{11}^e(t)^{(4)} &\approx -\frac{\Omega_1\Omega_2t^2}{8}(\mathcal{F}\{b_{00}^e(0)[1+i\zeta_1]-ib_{00}^e(0)\zeta_2\}(-\omega_1+\delta\omega)\mathcal{F}[1-i\zeta_1](-\omega_2-\delta\omega) \\
 &\quad -e^{-i2\phi_0}\mathcal{F}\{b_{00}^e(0)[1-i\zeta_1]-ib_{00}^e(0)\zeta_2^*\}(-\omega_1-\delta\omega)\mathcal{F}[i\zeta_2^*](-\omega_2-\delta\omega) \\
 &\quad +\mathcal{F}\{b_{00}^e(0)[1+i\zeta_1]-ib_{00}^e(0)\zeta_2\}(-\omega_2+\delta\omega)\mathcal{F}[1-i\zeta_1](-\omega_1-\delta\omega) \\
 &\quad -e^{-i2\phi_0}\mathcal{F}\{b_{00}^e(0)[1-i\zeta_1]-ib_{00}^e(0)\zeta_2^*\}(-\omega_2-\delta\omega)\mathcal{F}[i\zeta_2^*](-\omega_1-\delta\omega)). \tag{23}
 \end{aligned}$$

Due to the coefficients constituting a quickly decreasing series, the intermode photon cross correlation between two (ω_1, ω_2) high-order harmonic modes can be reasonably represented by

$$g_{12}(t) \approx \frac{|b_{11}^e|^2 + |b_{11}^g|^2}{(|b_{10}^e|^2 + |b_{10}^g|^2)(|b_{01}^e|^2 + |b_{01}^g|^2)},$$

where, during evaluation, it is worth separating the special cases below. For the sake of simplicity, we will consider only the initial condition $|g\rangle|0\rangle \dots |0\rangle$, which does not limit the validity of the conclusions.

Odd-odd harmonic modes. Let the frequencies be $\omega_1 = (2k_1 + 1)\omega$ and $\omega_2 = (2k_2 + 1)\omega$, where $k_1, k_2 \in \mathcal{N}$. Between two odd harmonic lines, the cross correlation is

$$g_{12}(t) \approx \frac{\frac{\Omega_1^2\Omega_2^2t^4}{64}|2e^{-i2\phi_0}\mathcal{F}[\zeta_2^*](-\omega_1-\delta\omega)\mathcal{F}[\zeta_2^*](-\omega_2-\delta\omega)|^2}{\frac{\Omega_1^2t^2}{4}|e^{-i\phi_0}\mathcal{F}[\zeta_2^*](-\omega_1-\delta\omega)|^2\frac{\Omega_2^2t^2}{4}|e^{-i\phi_0}\mathcal{F}[\zeta_2^*](-\omega_2-\delta\omega)|^2} = 1, \tag{24}$$

which is close to the numerically calculated value.

Even-even harmonic modes. Let us choose the frequencies as $\omega_1 = 2k_1\omega + \delta\omega$ and $\omega_2 = 2k_2\omega + \delta\omega$. Between such even harmonic lines, the cross correlation is

$$g_{12}(t) \approx \frac{\frac{\Omega_1^2\Omega_2^2t^4}{64}|\mathcal{F}[\zeta_1](-\omega_1+\delta\omega)\mathcal{F}[\zeta_1](-\omega_2-\delta\omega) + \mathcal{F}[\zeta_1](-\omega_1-\delta\omega)\mathcal{F}[\zeta_1](-\omega_2+\delta\omega)|^2}{\frac{\Omega_1^2t^2}{4}|e^{i\phi_0}\mathcal{F}[\zeta_1](-\omega_1+\delta\omega)|^2\frac{\Omega_2^2t^2}{4}|e^{i\phi_0}\mathcal{F}[\zeta_1](-\omega_2+\delta\omega)|^2} = 0. \tag{25}$$

We can check that the perturbative calculation predicts a nonclassical entanglement between even harmonic modes, since $\langle N_1N_2 \rangle = 0 < |b_{10}^g b_{01}^g|^2 = |\langle a_1 a_2^\dagger \rangle|$.

Odd-even harmonic modes. To calculate the correlation between odd and even harmonics, let us choose the mode frequencies as $\omega_1 = (2k_1 + 1)\omega$ and $\omega_2 = 2k_2\omega + \delta\omega$,

$$g_{12}(t) \approx \frac{\frac{\Omega_1^2\Omega_2^2t^4}{64}|\mathcal{F}[\zeta_2^*](-\omega_1-\delta\omega)\mathcal{F}[\zeta_1](-\omega_2+\delta\omega) + e^{i2\phi_0}\mathcal{F}[\zeta_2](-\omega_1+\delta\omega)\mathcal{F}[\zeta_1](-\omega_2+\delta\omega)|^2}{\frac{\Omega_1^2t^2}{4}|e^{i\phi_0}\mathcal{F}[\zeta_1](-\omega_2+\delta\omega)|^2\frac{\Omega_2^2t^2}{4}|e^{-i\phi_0}\mathcal{F}[\zeta_2^*](-\omega_1-\delta\omega)|^2} = 0, \tag{26}$$

and, as above, there is nonclassical entanglement between even and odd harmonic modes.

C. Quantum state of the scattered field

We stress that the above approximate results can only be considered valid for monochromatic excitation and for a given set of parameters, for which $|\delta\omega|$ is maximal. (That is, for the special case that can be considered optimal for the creation of one-photon states.) By collecting the analytically gained results to reconstruct the quantum state of the scattered electromagnetic field (within the given approximations), we can write

$$\begin{aligned}
 |\Psi\rangle_{HH} &\sim c_o|\alpha_{3\omega}\rangle|\alpha_{5\omega}\rangle \dots |\alpha_{(2k+1)\omega}\rangle \\
 &\quad + c_e^1|\beta_{2\omega+\delta\omega}\rangle + c_e^2|\beta_{4\omega+\delta\omega}\rangle \dots + c_e^k|\beta_{2k\omega+\delta\omega}\rangle.
 \end{aligned}$$

Here, we only denoted those modes that are in a significantly different state than the vacuum, and $|\alpha\rangle$ is a coherent state, while $|\beta\rangle$ denotes a superposition of $|0\rangle$ and $|1\rangle$.

We note that the quantum state of the odd harmonics and even the anticorrelations between odd and even harmonic photons can be generalized for all monochromatic excitations, and even for pulsed excitations (at least to those that we investigated). However, the quantum state of even harmonic modes and the correlations between them strongly depends on the excitation parameters.

VI. ON QUANTIZED EXCITATION

In this section, the quantized nature of the excitation is incorporated into calculational schemes. Instead of containing

the time-dependent semiclassical $\Omega(t)$ term, the excitation in the Hamiltonian (4) is represented as a set of quantized modes, with coherent states as the initial condition. For this system, we apply the transformation

$$D_{\text{Exc}} \equiv \prod_{n \in \text{Exc}} D_n(\alpha_n e^{-i\omega_n t}) \|\Psi\rangle' = D_{\text{Exc}}^\dagger |\Psi\rangle, \\ H'_{qq} = D_{\text{Exc}}^\dagger H_{qq} D_{\text{Exc}} + i\hbar D_{\text{Exc}} \partial_t D_{\text{Exc}}^\dagger. \quad (27)$$

The value of α_n in the above transformation is determined by the spectral composition of the excitation. After simplifications, the Hamiltonian can be reduced to

$$H'_{qq} = \hbar \frac{\omega_0}{2} \sigma_z + \sum_{n \in \text{HH}} \hbar \left(\omega_n a_n^\dagger a_n + \frac{\Omega_n}{2} \sigma_x (a_n^\dagger + a_n) \right) \\ + \sum_{n \in \text{E}} \hbar \left(\omega_n A_n^\dagger A_n + \frac{\Omega_n}{2} \sigma_x (A_n^\dagger + A_n) \right) - \frac{\Omega(t)}{2} \sigma_x. \quad (28)$$

Naturally, the driving term $\Omega(t)$ that dominates the time evolution of the harmonics is unaffected by the quantum state of the excitation. At the same time, this term drives the base harmonic mode(s)—that is, the modes corresponding to the excitation—as well, and (considering that the interaction is resonant) the backaction on the excitation can be significant.

A. Backaction of HHG on quantized excitation

During the interaction, the photon statistical properties of the excitation modes are dynamically changing. While this (in our experience) has minor effect on the high harmonic spectrum, the modifications taking place in the quantum state of the excitation can be nevertheless experimentally relevant.

We calculated backaction on a single monochromatic excitation. Our results show that the modification is comparatively small if the parameters are chosen in such a way that $|\delta\omega|$ is extremal. For this perceived behavior, we give an approximate analytic explanation by neglecting the high harmonic modes.

Without the harmonics, the Hamiltonian reduces to

$$H'_{qq} = \hbar \frac{\omega_0}{2} \sigma_z + \hbar \left(\omega a^\dagger a + \frac{\Omega}{2} \sigma_x (a^\dagger + a) + \frac{\Omega}{2} \sigma_x \underbrace{(\alpha^* e^{i\omega t} + \alpha e^{-i\omega t})}_{\frac{A}{2\Omega} (e^{i\omega t + \phi_0} + e^{-i\omega t - \phi_0})} \right). \quad (29)$$

By writing the quantum state as

$$|\Psi\rangle = e^{i\frac{A\epsilon}{2\omega} \sin(\omega t + \phi_0) \sigma_x} e^{\frac{i}{2}(\omega t + \phi_0) \sigma_z} e^{-\frac{i}{\hbar} t \epsilon_+} \sum_{j=0}^{\infty} b_j^e |\tilde{\epsilon}\rangle |j, \alpha e^{-i\omega t}\rangle e^{-ij\omega_n t} \\ + e^{i\frac{A\epsilon}{2\omega} \sin(\omega t + \phi_0) \sigma_x} e^{\frac{i}{2}(\omega t + \phi_0) \sigma_z} e^{-\frac{i}{\hbar} t \epsilon_-} \sum_{j=0}^{\infty} b_j^g |\tilde{g}\rangle |j, \alpha e^{-i\omega t}\rangle e^{-ij\omega_n t}, \quad (30)$$

the dynamical equations turn out to be

$$i\dot{b}_j^e(t) = \langle \tilde{\epsilon} | W(t) | \tilde{\epsilon} \rangle b_j^e(t) + \langle \tilde{\epsilon} | W(t) | \tilde{g} \rangle e^{i\frac{\epsilon_+ - \epsilon_-}{\hbar} t} b_j^g(t) + \frac{\Omega}{2} e^{i(\delta\omega t - \phi_0)} \sum_k \langle j | a + a^\dagger | k \rangle e^{-i\omega(k-j)t} b_k^g(t) \\ - \Omega \cos\theta e^{i\frac{\epsilon_+ - \epsilon_-}{\hbar} t} \cos(\omega t + \phi_0) \sum_k \langle j | a + a^\dagger | k \rangle e^{-i\omega(k-j)t} b_k^g(t) + \frac{\Omega}{2} \sin(2\theta) \cos(\omega t + \phi_0) \\ \times \sum_k \langle j | a + a^\dagger | k \rangle e^{-i\omega(k-j)t} b_k^e(t), \\ i\dot{b}_j^g(t) = \langle \tilde{g} | W(t) | \tilde{g} \rangle b_j^g(t) + \langle \tilde{g} | W(t) | \tilde{\epsilon} \rangle e^{-i\frac{\epsilon_+ - \epsilon_-}{\hbar} t} b_j^e(t) + \frac{\Omega}{2} e^{-i(\delta\omega t + \phi_0)} \sum_k \langle j | a + a^\dagger | k \rangle e^{-i\omega(k-j)t} b_k^e(t) \\ - \Omega \cos\theta e^{i\frac{\epsilon_- - \epsilon_+}{\hbar} t} \cos(\omega t + \phi_0) \sum_k \langle j | a + a^\dagger | k \rangle e^{-i\omega(k-j)t} b_k^e(t) - \frac{\Omega}{2} \sin(2\theta) \cos(\omega t + \phi_0) \\ \times \sum_k \langle j | a + a^\dagger | k \rangle e^{-i\omega(k-j)t} b_k^g(t).$$

The notations θ and ϵ_\pm are defined in the Appendixes. It is easy to check that, unlike in the case of harmonic modes, the dynamical equations regarding the excitation mode have a resonant term [proportional to $\sin(2\theta)$ above] already at first-order perturbation.

To quantify the backaction—that is, the difference from the initial coherent quantum state that develops over time—we use the weighted sum $B_A \equiv \sum_j j(|b_j^e|^2 + |b_j^g|^2)$. Since the (displaced) vacuum state corresponds to the initially coherent

state, B_A characterizes measures the components orthogonal to the coherent state.

Its evaluation, together with the above considerations, leads us to the following conclusion: the backaction can be maximalized if $\cos\theta$ is maximal, that is, when $\delta\omega = 0$, whereas for parameters which fulfill the $\cos\theta = 0$ condition, the backaction on the excitation is minimal. This can be observed in Fig. 10, where the dominant feature (besides the continuous growth) is the T -periodic oscillation. We note that

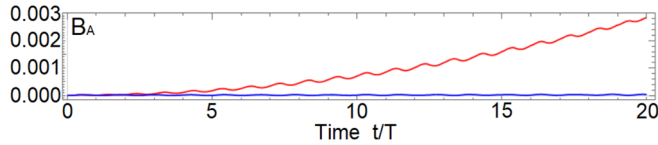


FIG. 10. Time evolution of the measure of backaction B_A . Parameters are chosen such that $\delta\omega$ is extremal (blue) and $\delta\omega = 0$ (red), with $\Omega/\sqrt{\omega} = 0.005$.

this oscillation largely corresponds to the periodical dynamics on phase space as described in [60].

B. Quantized excitation, quantized harmonics

Incorporating the fully quantum nature of the dynamics is numerically challenging without some kind of approximation. During our calculations, we employed the two-mode approximation, that is, considered only a single excitation and a single scattered mode.

A meaningful question, only treatable within the fully quantized formalism, is whether there are nontrivial correlations arising between absorption from the excitation mode and emission in the scattered modes.

Let us introduce an operator measuring the number of absorbed photons in the excitation mode:

$$\delta N \equiv |\alpha^2| - N. \quad (31)$$

We define the correlation function between δN and N_i as

$$g_{\delta i} \equiv \frac{\langle \delta N N_i \rangle}{\langle \delta N \rangle \langle N_i \rangle}, \quad (32)$$

which, unlike previously introduced correlation functions, can be of negative value, since δN can be negative. The parameters have been chosen so that the monochromatic excitation contains $\approx 10^8$ photons.

In Fig. 11(a) we can observe that photon absorption from the highly populated excitation mode happens in discrete steps in each half cycle. There is a nearly unit correlation between the absorption from excitation mode and emission in odd-harmonic modes [see Figs. 11(b) and 11(d)]; however, the even harmonic photon emissions are uncorrelated to the photon emission from the excitation [see Figs. 11(c) and 11(e)].

VII. CONCLUSIONS

We analyzed photon statistics of high-order harmonics specific to a two-level radiating system. The harmonics induced by monochromatic excitations follow a relatively simple behavior: odd harmonics oscillate between super-Poissonian and sub-Poissonian statistics, usually fulfilling the $Q \ll \langle N \rangle$ relation. Even harmonics (hyper-Raman lines) can be, depending on the parameters, either strongly squeezed or effectively in the superposition of zero- and one-photon states.

Our results point to the theoretical possibility that, with specific excitations, HHG can be the source of one-photon radiation in many modes, encompassing a broad spectral range (notably with detuning, the spectra can become quasicontinuum) or a source of broadband squeezed states.

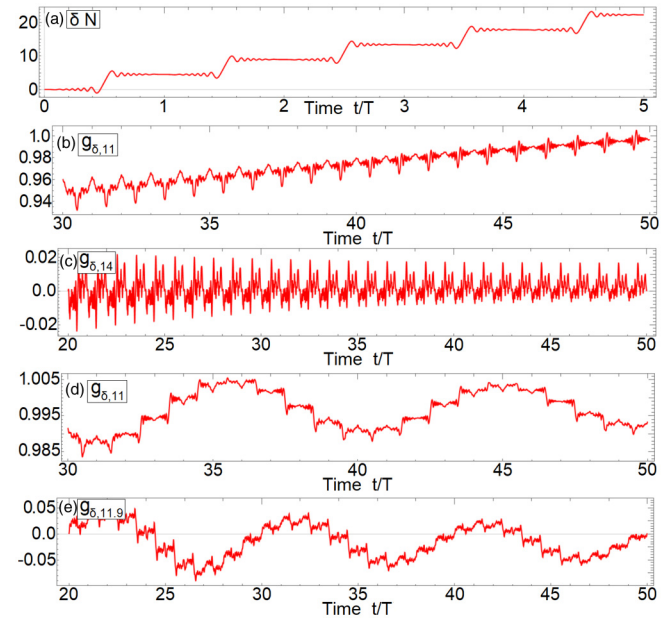


FIG. 11. Subfigure (a) shows time evolution of δN . Subfigures (b) and (c) show the correlation between the absorption of a photon in the excitation mode and the emission of a photon in an odd and even harmonic mode, respectively, with the parameter chosen so that $|\delta\omega| = 0$. Subfigures (d) and (e) are analogous, but with $|\delta\omega| = 0.1\omega$.

Intermodal correlations within the radiation field have also been investigated. Generally speaking, the odd-odd harmonic photons are classically cross correlated, while the odd- and even-harmonic photons are anticorrelated in all cases investigated by us. The even-even harmonic photons can be, depending on the parameters, either strongly correlated or anticorrelated. Our results suggest that the anticorrelations correspond to nonclassical entanglement.

In other words, we have found that nonclassical properties, potentially of experimental interest, can be associated primarily with the modes of even-order harmonics. HHG as a source of nonclassical light can be realized in the same experimental settings that allow observation of these optical lines; see, e.g., Ref. [59].

ACKNOWLEDGMENTS

This research was performed in the framework of Project No. GINOP-2.3.2-15-2016-00036. The project has also been supported by the European Union, cofinanced by the European Social Fund, Grant No. EFOP-3.6.2-16-2017-00005—Ultrafast physical processes in atoms, molecules, nanostructures, and biological systems. Support by the ELI-ALPS project is also acknowledged. The ELI-ALPS project (No. GINOP-2.3.6-15-2015-00001) is supported by the European Union and cofinanced by the European Regional Development Fund. We also acknowledge financial support from the Ministry of Innovation and Technology, Hungary, Grant No. NKFIH-1279-2/2020.

APPENDIX A: ANALYTICAL RESULT FOR CLASSICALLY DRIVEN TWO-LEVEL ATOM

The spectrum of scattered radiation from a two-level system under monochromatic excitation is structured into qualitatively different odd and even harmonics. While the two-level system has been investigated in the literature thoroughly using a semiclassical approach [61,62]—usually involving approximations that limit the validity of analytic results or given in a complicated form that offers little insight [63]—we present here a transparent analytic characterization of the dynamics with respect to HHG.

Consider the semiclassical H_{cc} Hamiltonian

$$H_{cc}(t) = \frac{\hbar\omega_0}{2}\sigma_z + \frac{\hbar A}{2}\sigma_x \cos(\omega t + \phi_0) \quad (\text{A1})$$

and use the unitary transformation

$$|\Psi'(t)\rangle = e^{\Lambda(t)}|\Psi(t)\rangle, \quad (\text{A2})$$

$$H'_{cc}(t) = e^{\Lambda(t)}H_{cc}e^{-\Lambda(t)} + i\hbar e^{-\Lambda(t)}\frac{\partial}{\partial t}e^{\Lambda(t)}, \quad (\text{A3})$$

with the choice

$$\Lambda(t) \equiv i\frac{A}{2\omega}\xi \sin(\omega t + \phi_0)\sigma_x. \quad (\text{A4})$$

Here $\xi \in \mathbf{R}$ is to be determined in the following. The transformed Hamiltonian can be written as

$$\begin{aligned} H'_{cc}(t) = & \frac{\hbar\omega_0}{2} \left\{ \cos\left[\frac{A}{\omega}\xi \sin(\omega t + \phi_0)\right]\sigma_z \right. \\ & \left. + \sin\left[\frac{A}{\omega}\xi \sin(\omega t + \phi_0)\right]\sigma_y \right\} \\ & + \frac{\hbar A}{2}(1 - \xi)\cos(\omega t + \phi_0)\sigma_x. \end{aligned} \quad (\text{A5})$$

Using the Anger-Jacobi identity, we can divide the Hamiltonian [64] as $H'_{cc}(t) = H'_0 + H'_1(t) + H'_2(t)$, where the terms are the following:

$$\begin{aligned} H'_0 &= \frac{\hbar\omega_0}{2}J_0\left(\frac{A}{\omega}\xi\right)\sigma_z, \quad (\text{A6}) \\ H'_1(t) &= \frac{\hbar A}{2}(1 - \xi)\cos(\omega t + \phi_0)\sigma_x. \end{aligned}$$

$$+ \hbar\omega_0 J_1\left(\frac{A}{\omega}\xi\right)\sin(\omega t + \phi_0)\sigma_y, \quad (\text{A7})$$

$$\begin{aligned} H'_2(t) = & \hbar\omega_0 \sum_{n=1}^{\infty} J_{2n}\left(\frac{A}{\omega}\xi\right)\cos[2n(\omega t + \phi_0)]\sigma_z \\ & + \hbar\omega_0 \sum_{n=1}^{\infty} J_{2n+1}\left(\frac{A}{\omega}\xi\right)\sin[(2n+1)(\omega t + \phi_0)]\sigma_y. \end{aligned} \quad (\text{A8})$$

With the neglect of $H'_2(t)$, a solution can be given [65]. However, as $H'_2(t)$ contains the terms associated with harmonic generations, we will need to incorporate it as the driving term in the interaction picture.

At this point, let us fix ξ such that

$$J_1\left(\frac{A}{\omega}\xi\right)\omega_0 = \frac{A}{2}(1 - \xi) \equiv \frac{B}{4}. \quad (\text{A9})$$

With this choice we can write

$$\begin{aligned} H'_0 + H'_1(t) &= \frac{\hbar\omega_0}{2}J_0\left(\frac{A}{\omega}\xi\right)\sigma_z + \frac{\hbar B}{4}(e^{-i(\omega t + \phi_0)}\sigma_+ + e^{i(\omega t + \phi_0)}\sigma_-). \end{aligned}$$

The solutions can be found straightforwardly by applying the rotation transformation $e^{\frac{i}{2}(\omega t + \phi_0)\sigma_z}$ and employing the $e^{\frac{i}{2}(\omega t + \phi_0)\sigma_z}\sigma_{\pm}e^{-\frac{i}{2}(\omega t + \phi_0)\sigma_z} = \sigma_{\pm}e^{\pm i(\omega t + \phi_0)}$ relation [66]. The transformed Hamiltonian and its eigenvalues turn out to be

$$\begin{aligned} \tilde{H}'_0 + \tilde{H}'_1 &= \frac{\hbar}{2}\left[\omega_0 J_0\left(\frac{A}{\omega}\xi\right) - \omega\right]\sigma_z + \frac{\hbar B}{4}\sigma_x, \\ \epsilon_{\pm} &= \pm \frac{\hbar}{2}\sqrt{\left[J_0\left(\frac{A}{\omega}\xi\right)\omega_0 - \omega\right]^2 + B^2/4}. \end{aligned} \quad (\text{A10})$$

The eigenvectors are

$$|\tilde{e}\rangle = \sin\theta|g\rangle + \cos\theta|e\rangle, \quad \|\tilde{g}\rangle = \sin\theta|e\rangle - \cos\theta|g\rangle,$$

where the θ parameter is given as

$$\theta = \arctan\left[\frac{\sqrt{\left[J_0\left(\frac{A}{\omega}\xi\right)\omega_0 - \omega\right]^2 + B^2/4} - \left[J_0\left(\frac{A}{\omega}\xi\right)\omega_0 - \omega\right]}{B/2}\right]. \quad (\text{A11})$$

The time evolution can then be understood on the basis of eigenstates $|\tilde{e}\rangle$ and $|\tilde{g}\rangle$ in the interaction picture. The driving is done by $\hbar W(t) \equiv e^{\frac{i}{2}(\omega t + \phi_0)\sigma_z}H'_2(t)e^{-\frac{i}{2}(\omega t + \phi_0)\sigma_z}$, where

$$W(t) = \omega_0 \sum_{n=1}^{\infty} J_{2n}\left(\frac{A}{\omega}\xi\right)\cos[2n(\omega t + \phi_0)]\sigma_z + \omega_0 \sum_{n=1}^{\infty} J_{2n+1}\left(\frac{A}{\omega}\xi\right)\sin[(2n+1)(\omega t + \phi_0)][\sin(\omega t + \phi_0)\sigma_x + \cos(\omega t + \phi_0)\sigma_y]. \quad (\text{A12})$$

The quantum state is written as

$$|\Psi\rangle = b^e(t)e^{i\frac{A\xi}{2\omega}\sin(\omega t + \phi_0)\sigma_x}e^{\frac{i}{2}(\omega t + \phi_0)\sigma_z}|\tilde{e}\rangle e^{-\frac{i}{\hbar}\epsilon_+ t} + b^g(t)e^{i\frac{A\xi}{2\omega}\sin(\omega t + \phi_0)\sigma_x}e^{\frac{i}{2}(\omega t + \phi_0)\sigma_z}|\tilde{g}\rangle e^{-\frac{i}{\hbar}\epsilon_- t}, \quad (\text{A13})$$

with the time dependence of coefficients b^e and b^g given by

$$ib^e(t) = \langle \tilde{e}|W(t)|\tilde{e}\rangle b^e(t) + \langle \tilde{e}|W(t)|\tilde{g}\rangle e^{-i\frac{\epsilon_- - \epsilon_+}{\hbar}t} b^g(t), \quad ib^g(t) = \langle \tilde{g}|W(t)|\tilde{g}\rangle b^g(t) + \langle \tilde{g}|W(t)|\tilde{e}\rangle e^{-i\frac{\epsilon_+ - \epsilon_-}{\hbar}t} b^e(t).$$

The physical picture emerging is the following: the eigenstates of $\tilde{H}'_0 + \tilde{H}'_1(t)$ define two energy levels, which together with the unitary transform define a set of infinite virtual energy levels (essentially equivalent to the Floquet quasienergies). At the same time, $\hbar W(t)$ corresponds to higher-order optical processes and induces transitions between the eigenstates.

Using the following formulae:

$$\begin{aligned} \langle \tilde{e} | \sigma_z | \tilde{e} \rangle &= \cos^2 \theta - \sin^2 \theta, & \langle \tilde{g} | \sigma_z | \tilde{g} \rangle &= \sin^2 \theta - \cos^2 \theta, & \langle \tilde{e} | \sigma_z | \tilde{g} \rangle &= \langle \tilde{e} | \sigma_z | \tilde{e} \rangle = 2 \sin \theta \cos \theta, \\ \langle \tilde{e} | \sigma_x | \tilde{e} \rangle &= 2 \sin \theta \cos \theta, & \langle \tilde{e} | \sigma_y | \tilde{e} \rangle &= 0, & \langle \tilde{g} | \sigma_x | \tilde{g} \rangle &= -2 \sin \theta \cos \theta, & \langle \tilde{g} | \sigma_y | \tilde{g} \rangle &= 0, \\ \langle \tilde{g} | \sigma_x | \tilde{e} \rangle &= \langle \tilde{e} | \sigma_x | \tilde{g} \rangle = \sin^2 \theta - \cos^2 \theta, & \langle \tilde{g} | \sigma_y | \tilde{e} \rangle &= -i = -\langle \tilde{e} | \sigma_y | \tilde{g} \rangle, \end{aligned}$$

the dynamical equations can be expanded, using the nonlinear optical parameter $\eta \equiv \frac{A\xi}{\omega}$ as below:

$$\begin{aligned} i\dot{b}^e(t) &= b^e(t)\omega_0 \sum_{n=1}^{\infty} \left[J_{2n}(\eta) \cos(2\theta) \cos[2n(\omega t + \phi_0)] + \frac{J_{2n+1}(\eta)}{2} \sin(2\theta) \{ \cos[2n(\omega t + \phi_0)] - \cos[(2n+2)(\omega t + \phi_0)] \} \right] \\ &+ b^s(t)\omega_0 e^{-i\frac{\epsilon_+ - \epsilon_-}{\hbar}t} \sum_{n=1}^{\infty} \left[J_{2n}(\eta) \sin(2\theta) \cos[2n(\omega t + \phi_0)] - \frac{J_{2n+1}(\eta)}{2} \cos(2\theta) \{ \cos[2n(\omega t + \phi_0)] \right. \\ &\left. - \cos[(2n+2)(\omega t + \phi_0)] \} + i\frac{J_{2n+1}(\eta)}{2} \{ \sin[(2n+2)(\omega t + \phi_0)] + \sin[2n(\omega t + \phi_0)] \} \right], \end{aligned} \quad (\text{A14})$$

$$\begin{aligned} i\dot{b}^s(t) &= -b^s(t)\omega_0 \sum_{n=1}^{\infty} \left[J_{2n}(\eta) \cos(2\theta) \cos[2n(\omega t + \phi_0)] + \frac{J_{2n+1}(\eta)}{2} \sin(2\theta) \{ \cos[2n(\omega t + \phi_0)] - \cos[(2n+2)(\omega t + \phi_0)] \} \right] \\ &+ b^e(t)\omega_0 e^{-i\frac{\epsilon_+ - \epsilon_-}{\hbar}t} \sum_{n=1}^{\infty} \left[J_{2n}(\eta) \sin(2\theta) \cos[2n(\omega t + \phi_0)] - \frac{J_{2n+1}(\eta)}{2} \cos(2\theta) \{ \cos[2n(\omega t + \phi_0)] \right. \\ &\left. - \cos[(2n+2)(\omega t + \phi_0)] \} - i\frac{J_{2n+1}(\eta)}{2} \{ \sin[(2n+2)(\omega t + \phi_0)] + \sin[2n(\omega t + \phi_0)] \} \right]. \end{aligned} \quad (\text{A15})$$

In semiclassical spectral calculations, the quantity of interest is $\langle D(t) \rangle \equiv \langle \Psi | d\sigma_x | \Psi \rangle$, the expectation value of the dipole moment:

$$\begin{aligned} \langle D \rangle / d &= [|b^+(t)|^2 - |b^-(t)|^2] \cos(\omega t + \phi_0) 2 \sin \theta \cos \theta \\ &+ 2 \operatorname{Re}[b^{+*}(t)b^-(t)e^{i\frac{\epsilon_+ - \epsilon_-}{\hbar}t}] \\ &\times \cos(\omega t + \phi_0)(\sin^2 \theta - \cos^2 \theta) \\ &+ 2 \operatorname{Im}[b^{+*}(t)b^-(t)e^{i\frac{\epsilon_+ - \epsilon_-}{\hbar}t}] \sin(\omega t + \phi_0). \end{aligned} \quad (\text{A16})$$

Evaluation shows that the terms with not odd-harmonic frequencies have (plus-minus) $\delta\omega \equiv \frac{\epsilon_+ - \epsilon_-}{\hbar} - \omega$ detuning from even-order multiples of the basic harmonic.

If we fix the gap ω_0 and detuning ω/ω_0 ratio, both $\cos \theta$ and $\delta\omega$ are functions of only the amplitude and are asymptotically (albeit with slow convergence) zero; see Fig. 12. Let us note that zero points of $\cos \theta$ are corresponding to local extremum of $\delta\omega/\omega$; that is, at these parameters the dual lines of even harmonics have maximal separation. The $\cos \theta$ function has zero

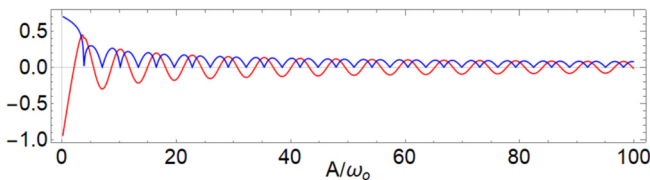


FIG. 12. Dependence of $\delta\omega/\omega$ (red) and $\cos \theta$ (blue) on the amplitude of resonant excitation.

points in all intensity range, more or less being distributed evenly.

APPENDIX B: FIRST-ORDER PERTURBATIVE EXPANSION

In the dynamical equations (A14) and (A15) there is no resonant contribution, that is, the $b^{(e/s)}$ coefficients follow high-frequency, small-amplitude oscillations around their initial values, which implies that perturbation methods are applicable. Comparison between spectra calculated numerically and through first-order perturbation—within realistic excitation intensity value—can be seen on Fig. 13. We note that the dominant spectral lines (odd or even harmonics, depending on the initial conditions) are reproduced by the perturbative treatment typically within $\sim 10\%$ relative error.

For the sake of simplicity, we focus on the special case of $\cos \theta = 0$, which, as mentioned above, corresponds to the maximal spectral gap between the dual lines of even harmonics. Then Eqs. (A14) and (A15) become

$$\begin{aligned} i\dot{b}^e(t) &= -b^e(t)\omega_0 \sum_{n=1}^{\infty} [J_{2n}(\eta) \cos[2n(\omega t + \phi_0)]] \\ &+ b^s(t)\omega_0 e^{-i\frac{\epsilon_+ - \epsilon_-}{\hbar}t} \sum_{n=1}^{\infty} \left[\frac{J_{2n+1}(\eta)}{2} \{ \exp[2ni(\omega t + \phi_0)] \right. \\ &\left. - \exp[-(2n+2)i(\omega t + \phi_0)] \} \right], \end{aligned}$$

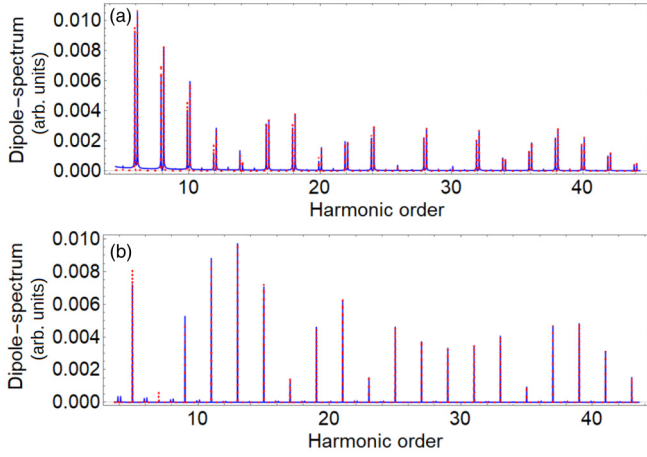


FIG. 13. Comparison of spectrum induced by resonant excitation, calculated numerically (blue) and with the first-order perturbation method (dashed). Subfigure (a) shows the spectra calculated with initial condition $b^e = b^s = 1/\sqrt{2}$ and (b) with initial condition $b^s = 1$.

$$\begin{aligned}
 i\dot{b}^s(t) = & b^s(t)\omega_0 \sum_{n=1}^{\infty} [J_{2n}(\eta) \cos[2n(\omega t + \phi_0)]] \\
 & + b^e(t)\omega_0 e^{-i\frac{\epsilon_+ - \epsilon_-}{\hbar}t} \sum_{n=1}^{\infty} \left[\frac{J_{2n+1}(\eta)}{2} \{ \exp[-2ni(\omega t + \phi_0)] \right. \\
 & \left. - \exp[(2n+2)i(\omega t + \phi_0)] \} \right].
 \end{aligned}$$

This special case is not unrealistic, considering that a careful selection of the parameters allows this condition to be fulfilled in all, not too specific intensity intervals.

Here we give the analytic expression of the first-order perturbation calculation results which have been employed in the article. The first-order perturbative solution can be

written as

$$\begin{aligned}
 b^e(t) & \approx b^e(0) + ib^e(0)\zeta_1(t) - ib^s(0)\zeta_2(t), \\
 b^s(t) & \approx b^s(0) - ib^s(0)\zeta_1(t) - ib^e(0)\zeta_2^*(t),
 \end{aligned} \quad (\text{B1})$$

where we define the $\zeta_1(t)$ and $\zeta_2(t)$ expressions as

$$\begin{aligned}
 \zeta_1(t) & = \omega_0 \sum_{n=1}^{\infty} \left[\frac{J_{2n}(\eta)}{2n\omega} \{ \sin[2n(\omega t + \phi_0)] - \sin[2n\phi_0] \} \right], \\
 \zeta_2(t) & = i\omega_0 \sum_{n=1}^{\infty} \left[\frac{J_{2n+1}(\eta)}{2} \left(\frac{[1 - e^{i(2n\omega + \frac{\epsilon_+ - \epsilon_-}{\hbar})t}]}{2n\omega + \frac{\epsilon_+ - \epsilon_-}{\hbar}} e^{i2n\phi_0} \right. \right. \\
 & \left. \left. + \frac{[1 - e^{i(-(2n+2)\omega + \frac{\epsilon_+ - \epsilon_-}{\hbar})t}]}{(2n+2)\omega - \frac{\epsilon_+ - \epsilon_-}{\hbar}} e^{-i(2n+2)\phi_0} \right) \right].
 \end{aligned}$$

The dipole-operator expectation value can be expressed through $b^{e*}(t)b^s(t)e^{i\frac{\epsilon_+ - \epsilon_-}{\hbar}t}$, which, after simplification, can be rewritten as (B2).

The evaluation of the dipole moment can be done in a lengthy but straightforward manner. The dipole oscillation contains frequencies $(2n+1)\omega$ and $(2n+1)\omega \pm \frac{\epsilon_+ - \epsilon_-}{\hbar} = (2n+2)\omega \pm \delta\omega$:

$$\begin{aligned}
 & b^{e*}(t)b^s(t)e^{i\frac{\epsilon_+ - \epsilon_-}{\hbar}t} \\
 & = b^{e*}(0)b^s(0)[1 - i\zeta_1(t)]^2 e^{i\frac{\epsilon_+ - \epsilon_-}{\hbar}t} \\
 & \quad + b^{s*}(0)b^e(0)[\zeta_2^*(t)]^2 e^{i\frac{\epsilon_+ - \epsilon_-}{\hbar}t} \\
 & \quad + [|b^s(0)|^2 - |b^e(0)|^2] [i\zeta_2^*(t) + \zeta_1(t)\zeta_2^*(t)] e^{i\frac{\epsilon_+ - \epsilon_-}{\hbar}t}.
 \end{aligned} \quad (\text{B2})$$

If either $b^s(0)$ or $b^e(0)$ is zero, we can expect the lack of even-order harmonics in semiclassical solutions. We note in passing that the two spectral lines within even harmonics carry different multiples of the excitation phase, which can have consequences when macroscopic wave propagation is considered.

-
- [1] M. Ferray, A. L'Huillier, X. F. Li, L. A. Lompre, G. Mainfray, and C. Manus, *J. Phys. B* **21**, L31 (1988).
- [2] M. Ivanov, R. Kienberger, A. Scrinzi, and D. Villeneuve, *J. Phys. B* **39**, 1 (2005).
- [3] C. Riek, P. Sulzer, M. Seeger, A. S. Moskalenko, G. Burkard, D. V. Seletskiy, and A. Leitenstorfer, *Nature (London)* **541**, 376 (2017).
- [4] G. Farkas and C. Tóth, *Phys. Lett. A* **168**, 447 (1992).
- [5] C. Brif, R. Chakrabarti, and H. Rabitz, *New J. Phys.* **12**, 075008 (2010).
- [6] L. V. Keldysh, *Sov. Phys. JETP* **20**, 1307 (1965).
- [7] F. Krausz and M. Ivanov, *Rev. Mod. Phys.* **81**, 163 (2009).
- [8] M. Lewenstein, P. Balcou, M. Y. Ivanov, A. L'Huillier, and P. B. Corkum, *Phys. Rev. A* **49**, 2117 (1994).
- [9] J. Bergou and S. Varró, *J. Phys. A* **14**, 1469 (1981).
- [10] S. Varró, *Photonics* **8**, 269 (2021).
- [11] I. Gonoskov, N. Tsatrafyllis, I. Kominis, and P. Tzallas, *Sci. Rep.* **6**, 32821 (2016).
- [12] N. Tsatrafyllis, I. Kominis, I. Gonoskov, and P. Tzallas, *Nat. Commun.* **8**, 15170 (2017).
- [13] N. Tsatrafyllis, S. Kühn, M. Dumergue, P. Földi, S. Kahaly, E. Cormier, I. A. Gonoskov, B. Kiss, K. Varju, S. Varro, and P. Tzallas, *Phys. Rev. Lett.* **122**, 193602 (2019).
- [14] T. Lamprou, R. Lopez-Martens, S. Haessler, I. Lontos, S. Kahaly, J. Rivera-Dean, P. Stammer, E. Pisanty, M. F. Ciappina, M. Lewenstein *et al.*, *Photonics* **8**, 192 (2021).
- [15] A. Goriach, O. Neufeld, N. Rivera, O. Cohen, and I. Kaminer, *Nat. Commun.* **11**, 4598 (2020).
- [16] S. Ghimire, A. D. DiChiara, E. Sistrunk, P. Agostini, L. F. DiMauro, and D. A. Reis, *Nat. Phys.* **7**, 138 (2011).
- [17] J. N. Heyman, K. Craig, B. Galdrikian, M. S. Sherwin, K. Campman, P. F. Hopkins, S. Fafard, and A. C. Gossard, *Phys. Rev. Lett.* **72**, 2183 (1994).

- [18] F. I. Gauthey, C. H. Keitel, P. L. Knight, and A. Maquet, *Phys. Rev. A* **52**, 525 (1995).
- [19] F. I. Gauthey, B. M. Garraway, and P. L. Knight, *Phys. Rev. A* **56**, 3093 (1997).
- [20] C. F. de Morisson Faria and I. Rotter, *Laser Phys.* **13**, 985 (2003).
- [21] A. Gombkötő, A. Czirják, S. Varró, and P. Földi, *Phys. Rev. A* **94**, 013853 (2016).
- [22] P. Földi, I. Magashegyi, A. Gombkötő, and S. Varró, *Photonics* **8**, 263 (2021).
- [23] M. Kira and S. W. Koch, *Semiconductor Quantum Optics* (Cambridge University Press, Cambridge, UK, 2011).
- [24] P. Földi, *Phys. Rev. B* **96**, 035112 (2017).
- [25] L. Mandel and E. Wolf, *Optical Coherence and Quantum Optics* (Cambridge University Press, Cambridge, UK, 1995).
- [26] A. Miranowicz, J. Bajer, W. Leonski, and R. Tanas, in *Fifth International Conference on Squeezed States and Uncertainty Relations* (NASA Conf. Publ., Washington, DC, 1998), pp. 427–434.
- [27] Y. Malakyan, *Opt. Commun.* **86**, 423 (1991).
- [28] K. Cahill and R. Glauber, *Phys. Rev.* **177**, 1857 (1969).
- [29] K. E. Cahill and R. J. Glauber, *Phys. Rev.* **177**, 1882 (1969).
- [30] B. Berne and G. Harp, *On the Calculation of Time Correlation Functions*, Advances in Chemical Physics Vol. 17 (Wiley, New York, 2007), pp. 63–227.
- [31] W. Bron, *Ultrashort Processes in Condensed Matter* (Springer, New York, 1993).
- [32] *Photomultiplier Tubes: Basics and Applications (Fourth Edition)* (Hamamatsu Photonics, Hamamatsu, 2017).
- [33] M. Aßmann, F. Veit, J.-S. Tempel, T. Berstermann, H. Stolz, M. van der Poel, J. Hvam, and M. Bayer, *Opt. Express* **18**, 20229 (2010).
- [34] I.-C. Benea-Chelmsu, C. Bonzon, C. Maissen, G. Scalari, M. Beck, and J. Faist, *Phys. Rev. A* **93**, 043812 (2016).
- [35] R. Hanbury Brown and R. Twiss, *Nature (London)* **178**, 1046 (1956).
- [36] R. Loudon, *The Quantum Theory of Light*, 2nd ed. (Oxford University Press, Oxford, 1982).
- [37] J. Peřina, *Quantum Statistics of Linear and Nonlinear Optical Phenomena* (Springer, New York, 1991).
- [38] S. Singh, *Opt. Commun.* **44**, 254 (1983).
- [39] X. T. Zou and L. Mandel, *Phys. Rev. A* **41**, 475 (1990).
- [40] J. Peřina, Z. Hradil, and B. Jurčo, *Quantum Optics and Fundamentals of Physics* (Kluwer Academic Publishers, Dordrecht, 1994).
- [41] C. C. Gerry and P. L. Knight, *Introductory Quantum Optics* (Cambridge University Press, Cambridge, UK, 2005).
- [42] P. Meystre and M. Sargent, *Elements of Quantum Optics*, 2nd ed. (Springer, New York, 1991).
- [43] A. Miranowicz, J. Bajer, H. Matsueda, R. Wahiddin, and R. Tanas, *J. Opt. B* **1**, 511 (1999).
- [44] A. Miranowicz, H. Matsueda, J. Bajer, R. Wahiddin, and R. Tanas, *J. Opt. B* **1**, 603 (1999).
- [45] A. Miranowicz, M. Bartkowiak, X. Wang, Y.-x. Liu, and F. Nori, *Phys. Rev. A* **82**, 013824 (2010).
- [46] H. Dung, A. Shumovsky, and N. Bogolubov, *Opt. Commun.* **90**, 322 (1992).
- [47] J.-S. Peng and G.-X. Li, *Introduction to Modern Quantum Optics* (World Scientific, Singapore, 1998).
- [48] M. Hillery and M. S. Zubairy, *Phys. Rev. Lett.* **96**, 050503 (2006).
- [49] D. F. Walls and G. J. Milburn, *Quantum Optics* (Springer, New York, 1994).
- [50] M. J. Collett and D. F. Walls, *Phys. Rev. A* **32**, 2887 (1985).
- [51] A. Lukš, V. Peřinová, and J. Peřina, *Opt. Commun.* **67**, 149 (1988).
- [52] L. Allen and J. H. Eberly, *Optical Resonance and Two-Level Atoms* (Dover, Mineola, NY, 1987).
- [53] B. Mollow, *Phys. Rev.* **188**, 1969 (1970).
- [54] M. Wegener, *Extreme Nonlinear Optics* (Springer, New York, 2005).
- [55] T. Tritschler, O. D. Mücke, M. Wegener, U. Morgner, and F. X. Kärtner, *Phys. Rev. Lett.* **90**, 217404 (2003).
- [56] T. Joyce and A. Jaron-Becker, in *APS Division of Atomic, Molecular and Optical Physics Meeting Abstracts* (APS, College Park, MD, 2019), p. S01.062.
- [57] T. Joyce and A. Jaron-Becker, *Opt. Lett.* **45**, 1954 (2020).
- [58] Y. Xia and A. Jaron-Becker, *Opt. Express* **24**, 4689 (2016).
- [59] E. Bloch, S. Beaulieu, D. Descamps, S. Petit, F. Légaré, A. Magunov, Y. Mairesse, and V. Strelkov, *New J. Phys.* **21**, 073006 (2019).
- [60] A. Gombkötő, S. Varró, P. Mati, and P. Földi, *Phys. Rev. A* **101**, 013418 (2020).
- [61] J. H. Shirley, *Phys. Rev.* **138**, B979 (1965).
- [62] B. M. Garraway and S. Stenholm, *Phys. Rev. A* **45**, 364 (1992).
- [63] Q. Xie and W. Hai, *Phys. Rev. A* **82**, 032117 (2010).
- [64] Y. Yan, Z. Lü, and H. Zheng, *Phys. Rev. A* **91**, 053834 (2015).
- [65] Z. Lü and H. Zheng, *Phys. Rev. A* **86**, 023831 (2012).
- [66] A. B. Klimov and S. Chumakov, *A Group-Theoretical Approach to Quantum Optics: Models of Atom-Field Interactions* (Wiley, New York, 2009).